

## Snow dynamics influence tree growth by controlling soil temperature in mountain pine forests



Alba Sanmiguel-Vallelado<sup>a,\*</sup>, J. Julio Camarero<sup>a</sup>, Enrique Morán-Tejeda<sup>b</sup>, Antonio Gazol<sup>a</sup>, Michele Colangelo<sup>a,c</sup>, Esteban Alonso-González<sup>a</sup>, Juan Ignacio López-Moreno<sup>a</sup>

<sup>a</sup> Pyrenean Institute of Ecology, CSIC (Spanish Research Council), Avda. Montaña 1005, 50005 Zaragoza, Spain

<sup>b</sup> Department of Geography, University of the Balearic Islands, Carr. de Valldemossa km 7.5, 07122 Palma de Mallorca, Spain

<sup>c</sup> School of Agricultural, Forest, Food and Environmental Sciences, University of Basilicata, viale dell'Ateneo Lucano 10, 85100 Potenza, Italy

### ARTICLE INFO

**Keywords:**

Pyrenees  
snow cover  
soil temperature  
subalpine forests  
tree growth  
xylogenesis

### ABSTRACT

Snow dynamics are key to understanding tree growth in mountain forests and future response to climate change. However, precise monitoring of microclimate conditions and variables related to tree growth and functioning are lacking. To advance on those issues, snow cover and microclimate conditions, tree phenology, xylogenesis, intra-annual radial growth and the concentration of sapwood and needle non-structural carbohydrates were intensively monitored in four *Pinus uncinata* forests along an altitudinal gradient over three years in a Pyrenean valley (NE Spain). Snow dynamics exerted strong influence on soil temperature and moisture, particularly before and during the early growing season. Soil temperature was the most relevant microclimate variable during the overall xylogenesis, mainly influencing the production of mature tracheids. Large snow accumulation resulted in later snow depletion and a consequent delay in soil warming onset. Low soil temperatures in the spring, related to prolonged snow persistence, retarded cambial reactivation and led to lower growth rate. Despite strong spatial variability among plots, wood production was determined by snow dynamics in three out of the four studied plots. This study highlights the major role played by early and late growing season soil temperatures on radial growth of mountain conifers. The results of this study suggest that a future shallower and more transitory snowpack in the studied forests, together with warmer soil and air temperatures, may increase radial growth and productivity of similar mid-latitude, young mountain forests.

### 1. Introduction

Climate plays a major role as driver of forest productivity, stem wood formation and radial growth (Babst et al., 2019). In mountainous areas, regional climate is greatly controlled by topographic complexity (elevation, aspect, slope) and also by the presence of forest patches, resulting in the creation of large microclimatic variability (Albrich et al., 2020; Dan Moore et al., 2005). In cold, high-elevation forests and alpine treelines, low air and soil temperatures limit tree growth by shortening the growing season and reducing growth rates (Körner, 2012). There is a minimal air temperature threshold for cambial activity of many conifers around 5°C (Rossi et al., 2008). Air temperatures can also impact tree growth by retarding or accelerating snowmelt (Barnett et al., 2005). Snow dynamics have been reported to influence forest productivity, radial growth and xylogenesis in subalpine and subarctic forest ecosystems (Carlson et al., 2017; Helama et al., 2013). A deep snowpack, together with low air

temperatures, can delay the melt-out date, resulting in later soil warming, delayed root growth and cambial onset, thus reducing growth (Kirdyanov et al., 2003; Rossi et al., 2011; Vaganov et al., 1999). Other studies, however, have not found that soil temperature strongly influences stem growth and, in such cases, air temperature was considered to be the main factor limiting xylogenesis (D'Orangeville et al., 2013; Lüpi et al., 2012; Rossi et al., 2007). Additionally, snowmelt enhances water infiltration into deep soils (Woelber et al., 2018) and can positively influence tree growth by reducing soil moisture-limitation in seasonally dry mountain areas from mid to low latitudes (St. George, 2014; Watson and Luckman, 2016; Zhang et al., 2019).

Mountain forests from mid to high latitudes, where growth is mainly controlled by low temperatures, are very exposed to climate warming (Albrich et al., 2020). Rising air temperatures are expected to promote tree growth by extending the growing season and increasing growth rates (Camarero et al., 2017; Zhang et al., 2017). A likely shallower shorter-lived snowpack in mid-latitude mountain ranges

\* Corresponding author.

E-mail address: [albasv@ipe.csic.es](mailto:albasv@ipe.csic.es) (A. Sanmiguel-Vallelado).

(Beniston, 2012; McCabe and Wolock, 2009; Morán-Tejeda et al., 2017; López-Moreno et al., 2017) will allow the soil temperature to rise earlier in the year, consequently prolonging the growing season. However, a shorter-lived snowpack may also lead to less available snowmelt water at the end of spring, intensifying periods of water shortage in drought-prone regions such as the Mediterranean mountains (Pederson et al., 2011; Truettner et al., 2018).

Understanding how snow dynamics affect tree growth in mountain forests will allow us to anticipate their future responses to forecasted climate change. That is especially relevant in the Spanish Pyrenees, which is a mountain range located in the transition of temperate-continent Atlantic-Euroasian and dry Mediterranean climate influences (Del Barrio et al., 1990; El Kenawy et al., 2011; López-Moreno et al., 2010; Morán-Tejeda et al., 2017). This study investigates how seasonal dynamics in snowpack characteristics modify microclimatic conditions (soil temperature and moisture) and tests if these modifications influence intra-annual growth and functioning in Mountain pine (*Pinus uncinata*). For that purpose, microclimate conditions, shoot and needle phenology, xylogenesis, radial growth, sapwood and needle non-structural carbohydrate (NSC) concentrations were monitored in four *P. uncinata* forests situated along altitudinal gradients over three consecutive years in a Pyrenean valley. The objectives of the study were (1) to determine the extent to which small-scale variations in soil temperature and moisture are influenced by snowpack magnitude and duration; (2) to characterize seasonal growth and functioning in *P. uncinata*; and (3) to analyze the influence of intra-annual snow dynamics on *P. uncinata* growth through snowpack contribution to microclimate. The main hypothesis is that snow dynamics influence intra-annual growth patterns through their impact on soil temperature and moisture.

## 2. Data and methods

### 2.1. Study species

The Mountain pine (*Pinus uncinata* Ram.) is a long-lived and shade-intolerant conifer which dominates in high-elevation areas of the Pyrenees, western Alps, and Iberian System (Cantegrel, 1983). Spain's geographical distribution is limited to the subalpine forests of the Pyrenees (1600 - 2500 m) and to two isolated populations in the Iberian System, where it reaches its southern distribution limit (Ruiz de la Torre and Ceballos, 1979). *P. uncinata* begins to form the annual tree ring in April-May and ends growing in October, with main growth peaks from May to July (Camarero et al., 1998). A positive effect of warm air temperatures during the autumn before ring formation and during the growing season has been widely reported in tree-ring studies. (Andreu et al., 2007; Camarero et al., 1998; Galván et al., 2014; Tardif et al., 2003). In addition, there is evidence that a preceding abundant snowpack negatively influences *P. uncinata* radial growth at inter-annual scale (Sanmiguel-Vallelado et al., 2019).

### 2.2. Study site

The study was performed in the central Spanish Pyrenees (Figure 1a), where climate is continental (Del Barrio et al., 1990). The experimental setting comprised four forest stands located in the Balneario de Panticosa valley (Figure 1b); all stands have different elevations (from 1674 to 2104 m a.s.l.), exposure, forest structure and microclimatology because of the complex topography in this area (see Table 1 and Figure 1c). During the study period, the average annual sum of precipitation registered in the valley bottom (1630 m) was 1493 mm. In each forest an experimental plot of approximately 450 m<sup>2</sup> was designed. The plots were labeled (plot 1, plot 2, plot 3 and plot 4) based on their locations in the valley (from N to S). *P. uncinata* dominates the studied stands, although plot 3 contained a few individual *Pinus sylvestris* L. At each experimental plot, five young individual *P. uncinata*

were monitored and their diameter at breast height (Dbh<sub>0</sub>) and full height were measured using tapes and clinometers, respectively.

### 2.3. Data collection

A graphical description of the monitoring procedures and measures variables is shown in Figure A.1.

#### 2.3.1. Microclimate data

Air temperature (T) and humidity (H) series were obtained using dataloggers (Tinytag-Plus-2; model TGP-4017, Gemini DataLoggers UK Ltd., Chichester, West Sussex, UK) that were equipped with naturally ventilated radiation shields (Datamate ACS-5050 Weather Shield; Gemini DataLoggers UK Ltd., Chichester, West Sussex, UK). One datalogger was installed at each plot stand, hanging from a tree branch, and measurements were recorded every 15 minutes from November 2015 to December 2018.

The soil temperature (T soil) series was obtained using miniature temperature loggers (Thermochron iButton; DS-1922L model, Dallas Semiconductors, Texas, USA). Four to six dataloggers were installed at each studied forest stand in a distributed manner, covering both forest openings and beneath forest canopy areas. The dataloggers were wrapped with laboratory film and duct tape to prevent corrosion, tied to metallic picks to facilitate their later retrieval, and buried in the ground at a depth of 10 – 20 cm. Soil temperature data were collected every hour from November 2015 to December 2018.

The soil moisture series was obtained using ECH<sub>2</sub>O probes (EC-5 model, Decagon Devices, Pullman, WA, USA). Soil moisture sensors were installed in a distributed manner at each plot: two sensors were installed in forest openings and two beneath forest canopy areas. Sensors were buried in the ground at a depth of 10 - 20 cm. Volumetric water content (VWC) of soil was registered by the ECH<sub>2</sub>O datalogger every 1.5 hours from November 2015 to December 2018. The first month of measurements was discarded in order to ensure a proper settling time after field installation.

Snowpack data were collected from November 2015 to June 2018. Each year comprised snow data collected from the onset of snow accumulation to the end of melting. The snow depth series was obtained from automatic time-lapse cameras (Bushnell, Trophy Cam, Kansas, USA) shooting every day at eight fixed snow poles at each plot: three poles were placed in an open area and five were placed beneath the forest canopy at each plot. Photographs were processed using ImageJ software (Rasband, 1997) to manually obtain a daily snow depth series. The average daily snow depth series for the set of poles at each experimental plot was calculated. Snow Water Equivalent (SWE) was manually surveyed every 10 to 15 days using a snow cylinder and scale (ETH core sampler, Swiss Federal Institute of Technology, Zurich) at snow pits dug at two single locations in each plot, one in a forest opening and one below the forest canopy. Two replicates per location were collected. Snow density data was calculated from SWE collected data using the equation (Eq. 1):

$$\rho_s = \frac{SWE \cdot \rho_w}{H} \quad (1)$$

where  $\rho_s$  is the snowpack density (kg·m<sup>-3</sup>), SWE is the measured equivalent water of the snowpack (m), H is the measured snowpack depth (m), and  $\rho_w$  is the assumed water density (kg·m<sup>-3</sup>). Daily snow density series were estimated by linear interpolation between each pair of density measurements from consecutive surveys. Daily SWE series for the set of poles at each experimental plot were inferred from data on daily snow depth and estimated daily snow density. The methodology to obtain the snow dataset is described in Sanmiguel-Vallelado et al. (2020).

#### 2.3.2. Stem radius variations

Changes in stem perimeter were monitored on two to three

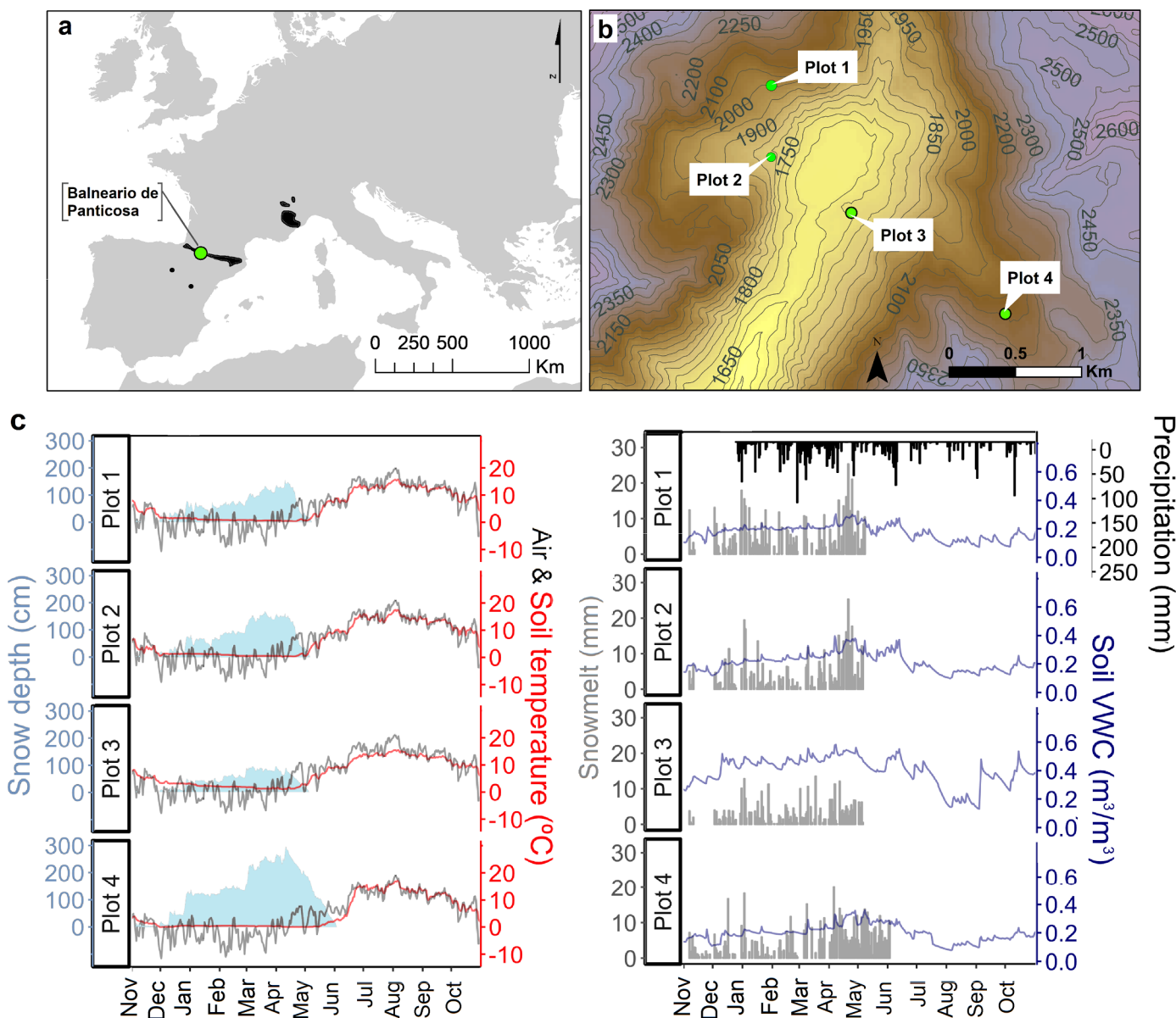


**Figure 1.** (a) Distribution of the study species (*Pinus uncinata*) in Europe (black areas) and location of the study area location (Balneario de Panticosa) in the Spanish Pyrenees (green dot). (b) Location of the experimental plots in the study valley. (c) On the left: daily time series of snow depth (light blue areas), mean soil temperature (red lines) and mean air temperature (grey lines) by plot during 2018. On the right: daily time series of snow melting rates (grey bars), mean soil VWC (blue lines), and precipitation sum (black bars) by plot during 2018. Precipitation data source was a meteorological station located in the study area at 1630 m a.s.l. (note that this series contained NA periods).

individual *P. uncinata* at each plot, using stainless-steel band dendrometers (DR 26, EMS Brno, Czech Republic). Dendrometers ( $n = 10$ ) were installed at a height of  $\sim 150$  cm on the individual stems. The external layer of dead bark was previously removed. Hourly stem

perimeter variations data (1  $\mu\text{m}$  resolution) were collected from April 2016 to December 2018 and transformed into radial changes, assuming a circular shape of the stem and measuring the diameter at breast height (1.3 m) at the beginning of the study ( $\text{Dbh}_0$ ). Data downloading

**Table 1**

Topography, microclimate conditions, tree characteristics, and forest structure in the four plots. Mean  $\pm$  standard deviations are presented.

Plot	Elevation (m a.s.l.)	Aspect	Slope (°)	DJF air T (°C)	TGS air T (°C)	Max SD (cm)	MAM GSI (W·m <sup>-2</sup> )	Dbh <sub>0</sub> (cm)	Height (m)	Age (years)†	Density (indiv·ha <sup>-1</sup> )	Basal area (m <sup>2</sup> ·ha <sup>-1</sup> )
1	2008	S	29.4	-0.5	11.1	133.2	154	$20.4 \pm 4.0$	$9.2 \pm 0.3$	$38 \pm 6$	1689	45.1
2	1814	E	20.4	-0.4	11.4	169.3	168	$18.8 \pm 4.6$	$8.6 \pm 1.2$	$35 \pm 7$	844	13.7
3	1674	W	9.3	0.3	12.2	95.3	193	$22.4 \pm 2.9$	$9.5 \pm 1.1$	$42 \pm 4$	533	35.3
4	2104	NE	22.7	-2.0	10.3	260.4	195	$20.2 \pm 4.0$	$9.1 \pm 0.3$	$37 \pm 6$	356	26.6

Abbreviations: DJF T, winter mean air temperature from December to February; TGS, Thermal Growing Season (see 2.4 section); Max SD, maximum snow depth; MAM GSI, average global solar irradiation from March to May; Dbh<sub>0</sub>, diameter at breast height at the beginning of the study. Note: The methods used to obtain stand structure data were described in Sanmiguel-Vallelado et al., (2020). (†) Tree age was estimated from Dbh<sub>0</sub> values based on an age-Dbh linear regression constructed in a nearby *P. uncinata* forest.

(Mini 32 software, EMS Brno, Czech Republic) was done seasonally (i.e. four times per year, every three months).

### 2.3.3. Xylogenesis

To study xylogenesis (xylem phenology and development), wood samples (microcores of 2 mm diameter and 15–20 mm length) were collected from five individual *P. uncinata* at each plot to monitor wood formation. Microcores ( $n = 20$ ) were taken weekly or bi-weekly from May to October during 2016 and 2017. The individuals were punched with a Trephor® increment puncher at 1–1.5 m height, following an ascending spiral pattern, and each sample was taken at least 5 cm from previous sampling points (Deslauriers et al., 2015). The samples usually contained the preceding 4–5 rings and the developing ring with the cambial zone and adjacent phloem. Microcores were immediately fixed in 50% ethanol solution and preserved.

Transversal wood sections (15–20  $\mu\text{m}$  thick) were obtained using a sliding microtome (Leica SM2010 R) with temperature Controlled Freezing Stages for Microtomes (Physitemp BFS-30MP), which allowed freezing the samples for optimal sectioning. Sections were mounted on glass slides, stained with 0.05% cresyl violet and fixed with Eukitt®. The mounted and fixed sections were examined with visible and polarized light within 10–30 min of staining. Images of sections were first taken at 40–100x magnification, using a digital camera mounted on a light microscope (Olympus BH2, Olympus, Hamburg, Germany). We counted and averaged, on five radial lines per ring, the number of cambium cells, radially enlarging tracheids, wall-thickening tracheids and mature cells (Camarero et al., 2010; Deslauriers et al., 2015). Images allowed verifying cell counts and distinguishing earlywood (EW) and latewood (LW) tracheids according to their lumen and cell wall thickness, distinguishing earlywood from latewood tracheids as a function of their radial lumen diameter and wall thickness following (Denne, 1989). In the developmental stage, cells showed different shapes and stained with different colors (Antonova and Stasova, 1993); cambial cells had similar and small radial diameters and thin walls; radially elongating tracheids showed a wider radial diameter and contained a protoplast enclosed by a thin primary wall; wall-thickening tracheids corresponded to the onset of secondary cell wall formation and were characterized by cell corner rounding; secondary walls glistened under polarized light and walls turned blue due to wall lignification; and mature cells did not contain cytoplasm and presented completely blue walls.

### 2.3.4. Shoot and needle phenology

Following the procedure reported in Rossi et al. (2009) the dynamics of shoot and needle growth on five individual *P. uncinata* were monitored at each experimental plot. Shoot and needle measurements were taken weekly or bi-weekly from May to October during 2016 and 2017. Five lower branches, from all exposures, were selected on each tree. On the branches, the developing apical shoots were measured with a ruler (1 mm precision). On each shoot, five developing needles were randomly selected and measured.

### 2.3.5. Non-structural carbohydrate concentrations

Non-structural carbohydrate (NSC) concentrations were quantified in stem sapwood and young needles of stems from individual five *P. uncinata* at each experimental plot. Three apical shoots and one core, taken at breast height (1.3 m) with Pressler increment borers (Gestern, Germany), were seasonally collected from selected trees in 2016. The concentrations of soluble sugars (SS) and starch (as non-soluble sugars NS) were measured in current-year needles and stem sapwood. Following Sangüesa-Barreda et al. (2012), SS were extracted with 80% ethanol solution and a colorimetric approach to determine their concentration. The undissolved fraction of carbohydrates after ethanol extraction was enzymatically reduced to glucose and then analyzed, as in Palacio et al. (2007). NSC measured after ethanol extraction is referred to as SS; carbohydrates measured after enzymatic digestion in glucose equivalents are referred to as starch; and the sum of SS and

starch is referred to as total NSC (TNC).

### 2.4. Data analyses

From the raw microclimate series, a few (<1%) outliers caused by errors in sensor measuring were removed. Missing data were estimated using a non-parametric iterative imputation method called missForest (Stekhoven and Bühlmann, 2012), which is implemented in the MissForest R package (Stekhoven, 2013). For each variable, the missForest method fits a Random Forest regression to the observed part and then predicts the missing parts of the input data (Breiman, 2001). Average daily series at each experimental plot were calculated. Data from forest openings and beneath forest canopy areas were averaged for SWE, soil temperature and soil moisture series. Snowmelt was calculated by first-order differencing from SWE daily series. Only snow data in a continuous snowpack period were considered; that is, from the date of the first day of 14 or more consecutive days with snow on the ground (i.e. snow accumulation onset) to the last date with a snow record (i.e. melt-out date). Air warming onset was defined as the day when the 7-day running mean air T reached a threshold of 5°C after the date of minimum air T, because 5°C is the minimal temperature threshold for cambial activity of many conifers (Rossi et al., 2008). Soil warming onset was determined the same way, with the soil temperature series. Therefore, the most favorable thermal growing season (TGS) comprises the period when air temperatures overcome the 5°C threshold. Snowmelt infiltration in soil was assumed when there was a rise of 0.01  $\text{m}^3 \cdot \text{m}^{-3} \cdot \text{day}^{-1}$  of soil VWC (Harpold et al., 2015).

Regressions at plot level (i) were performed between monthly sums of snowmelt and monthly averages of soil VWC and (ii) between monthly averages of SWE and soil T to investigate influences of snowpack on soil conditions. Linear and polynomial adjustments were done, respectively. The linear soil VWC response to snowmelt allowed inference of temporal variability of this relationship by performing correlation analysis between snowmelt weekly sums and soil VWC weekly averages, grouping by month and plot. The influence of snow duration on soil T over time was determined by performing correlation analysis between the melt-out date and the (current and following) monthly average values of soil temperature by plot and year.

From xylem development data, the increase in the number of mature tracheids was modelled at plot level with a Gompertz function (Eq. 2) (Zeide, 1993) using the non-linear regression procedure included in the growthmodels R package (Rodríguez Pérez, 2013), following Camarero et al. (1998) and Rossi et al. (2003).

$$Y = A * \exp[-\exp(\beta - k*t)] \quad (2)$$

where Y is the weekly cumulative sum of mature cells (sum of earlywood and latewood mature tracheids), A is the upper growth asymptote,  $\beta$  is the x-axis placement parameter,  $k$  is the rate of change parameter, and  $t$  is the time in day-of-year (DOY). Adjusted functions were again limited to the main *P. uncinata* growing season period (Camarero et al., 1998). Daily rates of mature tracheids production (Number of mature tracheids  $\cdot \text{day}^{-1}$ ) were estimated by first-order differencing the values of two consecutive days of the Gompertz-adjusted series.

For the stem radius variations data series, calculating daily mean and maximum values allows removal of the effect of temperature and soil moisture fluctuations on stem diameter changes over daily periods (Deslauriers et al., 2007). However, a daily approach was preferred because the temporal resolution of most available microclimate variables was not high enough to perform further analysis for selecting a stem cycle approach. Dendrometer raw data were processed using the dendrometeR package (van der Maaten et al., 2016) to obtain the daily

maximum radius series. Dendrometer data was delimited to the main *P. uncinata* growing period (Camarero et al., 1998), and was set to 0 on April 1 every season (in 2016 the series was set to 0 the May 1 due to data availability). Gompertz functions were adjusted to daily maximum radius series at plot level following the procedure described above (Eq. 2). Daily rates of radial increment ( $\mu\text{m}\cdot\text{day}^{-1}$ ) were estimated by first-order differencing the values of two consecutive days of the Gompertz-adjusted series. Some annual indices were extracted from mature tracheid production, stem radial increment and phenology data to characterize tree growth (see Table A.1).

Intra-annual microclimate effects on tree growth were examined by performing correlation analyses between weekly averages of microclimate variables and weekly maximum growth rates. Correlations were grouped by month and plot. Additionally, principal component analyses (PCA) were performed to identify the most representative microclimate variables of tree growth rates during the whole growing period. The first PCA was performed using weekly microclimate averages and maximum rates of mature tracheid production; the second PCA was performed using weekly microclimate averages and maximum rates of radial increment. A set of non-correlated variables (principal components, PCs) was obtained; these were linear combinations of the original variables (Jolliffe, 2002). The number of PCs selected in each PCA was based on the Kaiser criterion (Kaiser, 1974), preserving those with eigenvalues  $> 1$ . The original variables were classified into the selected PCs by following the maximum loading rule. Original variables were represented as vectors, indicating (i) the direction in which the value of the vector increases, and (ii) the correlation magnitude among vectors and between vectors and component axes (low angles correspond to high correlations).

The non-parametric Kruskal-Wallis test was used to assess whether there were statistically significant differences in certain variables among plots or years, (i.e. air and soil temperatures, soil VWC, and NSC concentrations). This test was selected because the assumption of normality in data distribution within the groups of analyzed variables was not always met (Shapiro-Wilk test:  $p < 0.05$ ). If the Kruskal-Wallis test was significant, the Dunn test post-hoc analysis was performed to determine which groups differed from each other. In correlations, Pearson coefficients were calculated when data distribution of the analyzed variables was normal (Shapiro-Wilk test:  $p > 0.05$ ), otherwise, Spearman coefficients were calculated. All analyses were performed using R statistical software (R Core Team, 2018).

### 3. Results

#### 3.1. Influence of snowpack on microclimate

Snow accumulation occurred from November to January, whereas the snow melt-out dates occurred throughout April and May (DOY  $122 \pm 21$ ; average value  $\pm$  SDs among all years and plots), with a snow cover lasting  $143 \pm 39$  days (Table A.2). Snow accumulation usually peaked in mid-March (DOY  $74 \pm 25$ ), reaching maximum depths of  $120 \pm 67$  cm. Larger snow accumulation involved later melt-out dates ( $r = 0.91, p < 0.05$ ) (Figure A.2) and a longer duration of annual snow cover ( $r = 0.87, p < 0.05$ ). More variability in snowpack duration and magnitude was found among plots ( $CV = 0.24, CV = 0.50$ ) than among years ( $CV = 0.16, CV = 0.29$ ).

Soil temperatures were highly influenced by snowpack magnitude during the snow-covered period. Both variables presented a non-linear relationship (Figure A.3); thus, snow presence induced soil cooling until insulation. Snowpacks with more than a 65 cm depth (on average) insulated the ground from winter air temperatures and, consequently, freezing of the soil surface was very rare. On average, soil temperature was  $3.3^\circ\text{C}$  higher than air temperature during winter. During spring, the snowpack also insulated the ground; in this case, soil temperature was on average  $2.8^\circ\text{C}$  lower than air temperature. Soil warming onset occurred in early May (DOY  $125 \pm 22$ ),  $4 \pm 8$  days after the melt-out

date, and  $26 \pm 23$  days after air warming onset (early April; DOY  $99 \pm 24$ ) (Table A.2). Soil warming onset differed among plots ( $SD = 18$  days), contrary to air warming onset ( $SD = 6$  days). Soil warming onset was driven by the melt-out date ( $r = 0.94, p < 0.05$ ; Figure A.2). May and June soil temperature was negatively influenced by melt-out date (Figure A.3). There were lagged effects (1–2 months) of snow persistence on soil temperature (in May  $r = -0.76, p < 0.05$ ; in June  $r = -0.71, p < 0.05$ ). Soil temperature also was correlated to air temperature during these months (in May:  $r = 0.69, p < 0.05$ ; in June:  $r = 0.66, p < 0.05$ ). From July onwards, soil temperature was mostly correlated to air temperature.

Soil water infiltration occurred during all snow-covered periods. Soil VWC peaked in late April (DOY  $120 \pm 17$ ),  $46 \pm 36$  days after the SWE peak, either before ( $2 \pm 28$  days) or after ( $23 \pm 27$  days) the melt-out date (Table A.2). No significant correlation was found in timing or magnitude between the soil VWC and SWE peaks. Positive relationships were found between snowmelt and soil VWC on a monthly scale (Figure A.4), being more frequent in Plot 1. This influence was stronger when larger melt occurred, i.e. in April and May (Figure A.4). No statistically significant correlations were found when lagged effects (1 or 2 months) of snowmelt on soil moisture were analyzed (data not shown).

Different microclimatic conditions were observed across plots and years (Table 1; Table A.2). Plot 4 showed the longest and thickest snowpacks, and the coldest air and soil temperatures during winter and TGS. Plot 3 showed the shortest and shallowest snowpacks, the warmest winter air temperature and TGS, and the highest soil VWC all year round. Plots 1 and 2 presented similar winter temperature and March snow depth. Plot 2 showed the warmest soil temperature during TGS. Plot 1 showed the lowest soil VWC values during TGS and reached the minimum soil VWC values earlier. In 2018, the longest and deepest snowpack, and the largest soil VWC and air humidity values during TGS were reached. In 2016, significantly warmer air and soil TGS temperatures were observed, whilst during 2017 the opposite was found. In 2017, the shortest snow season and, as a result, the earliest melt-out dates were observed.

#### 3.1. *uncinata* radial-growth characterization

Stem radial increment lasted on average  $91 \pm 44$  days; it began in mid-May (DOY  $130 \pm 15$ ) and finished in August (DOY  $221 \pm 33$ ) (Figure 2a; Table 2). Overall, the annual stem radial increment was  $1.0 \pm 0.7$  mm. More variability in the duration of the radial increment period was found among plots ( $CV = 0.40$ ) than among years ( $CV = 0.23$ ). More variability in seasonal radial change was also found among plots ( $CV = 0.75$ ) than among years ( $CV = 0.21$ ). Based on estimated daily rates of stem radial increment (Figure 2b, Table 2), growth peaked in mid-June (DOY  $162 \pm 9$ ). Again, more variability was found in the magnitude of maximum rates of radial increment among plots ( $CV = 0.49$ ) than among years ( $CV = 0.22$ ).

In 2018, the duration of the radial increment period was longer, the radial increment was higher and rates of radial increment were the lowest, followed by 2017. The maximum rates occurred earlier in 2017 than in other years. Plot 4 showed the longest radial increment periods, the highest and latest rates of radial increment and the largest total radial increment; followed primarily by plot 3. Plot 1 showed the lowest values for the mentioned variables.

The onset of tracheid formation, i.e. when the first enlarging tracheids were formed, occurred in mid-May (Figure 3a). The number of radially enlarging tracheids peaked from mid-May to late June. Tracheid maturation ended in October, when the thickening phase finished. Based on Gompertz models adjusted to the cumulative sum of mature cells, the estimated timing of growth season differed slightly from the previously noted (Figure 3b). The formation of mature tracheids started in early June (DOY  $160 \pm 7$ ) and finished in October (DOY  $286 \pm 20$ ) (Table 2). Maximum rates of production of mature tracheids ( $0.57 \pm 0.28$  cells  $\text{day}^{-1}$ ) occurred in mid-July (DOY  $202 \pm 20$ )

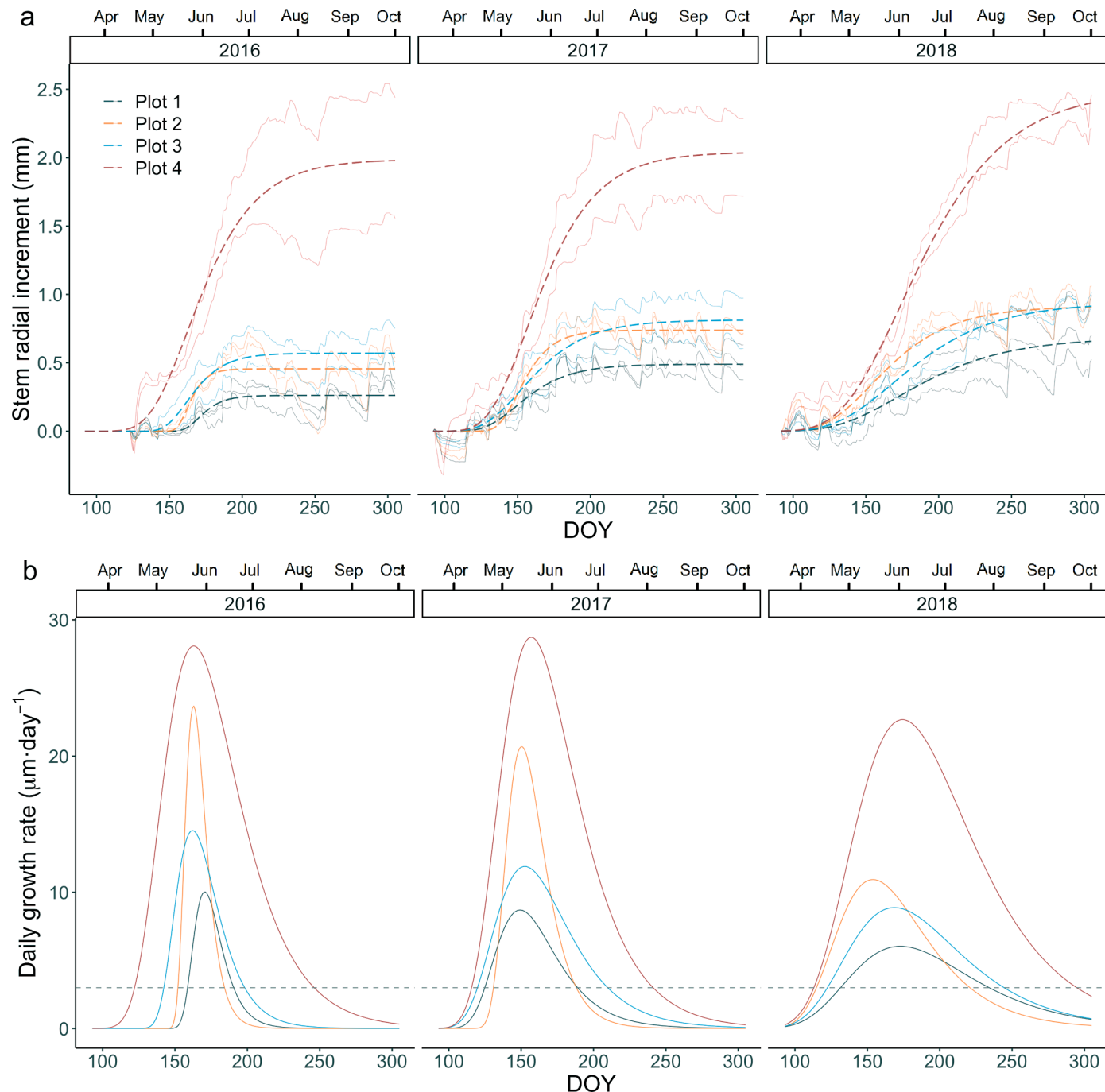


**Figure 2.** (a) Time series of stem daily maximum radius by tree (solid lines) and same series adjusted to Gompertz function at plot level (dashed lines) during 2016, 2017 and 2018. (b) Estimated daily rates of stem radial increment by plot during 2016, 2017 and 2018. Timing is represented by the day of the year (DOY). Dashed lines in the bottom panels represent daily growth rates equal to  $3 \mu\text{m}\cdot\text{day}^{-1}$ .

(Figure 3c). A high variability was found in the magnitude of maximum rates of production of mature tracheids among plots ( $CV = 0.51$ ), but not among years ( $CV = 0.17$ ).

The production of mature tracheids started and peaked earlier in 2017 but lasted longer in 2016 (Figure 3c). Plot 4 showed the longest period of production of mature tracheids, and the highest production rate, followed by plot 3, whereas plot 1 showed the lowest values for the mentioned variables.

### 3.2. Needle and shoot phenology

In 2016, the onset of shoot elongation occurred earlier (May) than

in 2017 (early June). A 55% smaller shoot length was reached in 2016 than in 2017 (Figure A.5.). For needles, the onset of elongation occurred later in 2016 (late June) than in 2017 (early June). A 15% longer needle was formed in 2016. The highest shoot and needle growth rates took place in plot 1, whilst the smallest rates were observed in plot 4.

### 3.3. Needle and sapwood non-structural carbohydrate (NSC) concentrations

Sapwood SS and starch concentrations peaked in October, whereas needle SS concentrations peaked in August or before (April, June). Needle starch concentrations peaked in June (plots 1 and 2), April (plot

**Table 2**

Growth characteristics considering stem radius increment and production of mature tracheids. Average values during 2016, 2017 and 2018 at each plot are shown.

Year	Plot	Stem radius increment					Mature tracheids						
		Total radial increment (mm·y <sup>-1</sup> )	Onset (DOY)	Cessation (DOY)	Duration (days)	Max rate (μm·d <sup>-1</sup> )	Timing of max rate (DOY)	Cell production (N° mature trach·y <sup>-1</sup> )	Onset (DOY)	Cessation (DOY)	Duration (days)	Max rate (n° mat trach·d <sup>-1</sup> )	Timing of max rate (DOY)
2016	1	0.26	159	191	32	10	171	30	163	297	134	0.23	221
	2	0.46	153	185	32	24	163	25	162	285	123	0.28	201
	3	0.57	143	199	56	15	162	70	162	302	140	0.62	222
	4	1.99	123	247	124	28	163	90	172	305	133	0.89	228
2017	1	0.49	125	189	64	9	149	21	161	246	85	0.42	182
	2	0.74	131	189	58	21	150	32	155	282	127	0.41	190
	3	0.81	120	210	90	12	153	35	151	272	121	0.76	172
	4	2.04	116	242	126	29	157	78	153	298	145	0.97	197
2018	1	0.69	132	235	103	6	173	—	—	—	—	—	—
	2	0.91	115	221	106	11	154	—	—	—	—	—	—
	3	0.94	123	245	122	9	169	—	—	—	—	—	—
	4	2.50	114	295	181	23	174	—	—	—	—	—	—

3) or October (plot 4). In 2016, maximum NSC concentrations in needles were reached in April in plot 4, June in plot 2 and August in plots 1 and 3 (Table 3). In sapwood, maximum TNC were reached in all plots in October. There was no significant difference in needle and sapwood NSC concentrations among plots.

#### 3.4. Microclimate influences on growth

Soil temperature was the microclimate variable most related to xylogenesis during June (when the first mature tracheids were observed) and September (during the final phase of tracheid maturation) (Figure 4a). The positive influence of soil temperature on growth mainly occurred throughout the entire spring. Soil temperatures (7-day mean) were  $10.4 \pm 1.4$  °C and  $7.9 \pm 2.8$  °C when the first and last mature tracheids were formed, respectively. A later soil warming onset can delay and therefore shorten the growing season, and this was related to a lower growth rate (see Figure A.6). This was observed in 3 out of the 4 studied plots, with plot 4 not showing this relationship. Air temperature showed positive correlations to xylem development rates in May, when the first radially enlarging tracheids were detected. Air and soil temperatures (7-day mean) were  $6.1 \pm 3.1$  °C and  $5.6 \pm 3.6$  °C, respectively, when the first radially enlarging tracheids were observed. Mostly negative correlations of xylem development rates with soil VWC were found during September and during the spring in plot 4. An exception was the positive correlation found in plot 1 with April soil VWC.

For radial increment rates, air temperature was the variable that most related to these rates during May in all plots (Figure 4b). In most plots, soil temperatures were also relevant to the onset of stem radial increment. Air and soil temperatures (7-day means) were  $8.4 \pm 4.5$  °C and  $5.9 \pm 4.7$  °C respectively, when the stem radial increment began. July air H and July-August soil VWC were positively correlated to stem radial increment rates in all plots. Maximum radial increment rates occurred about 10 days earlier ( $\pm 9$  days) than maximum day length.

The first principal component (PC1) of the first PCA explained 55.3% of the variability (Table A.3). Air T, soil T and xylem development rates spread along the PC1 axis increasing in same direction, while soil VWC increased in the opposite direction. Rates of production of mature tracheids were highly and positively related to soil temperature, followed by air temperature (Figure 5a). As air H spread along the second principal component (PC2), explaining only a small percentage of variability (18.16 %), its influence on formation of mature tracheids was low. The PC1 of the second PCA, performed considering all microclimate variables and radial increment rates, explained 49.9% of the variability. All microclimate variables spread along the PC1 axis, where air and soil T increased in the opposite direction of air H and soil VWC (Table A.3). Radial increment rates spread alone along the PC2 axis (22.1 %). Among microclimate variables, soil VWC was related to radial increment rates (Figure 5b), followed by air H.

#### 4. Discussion

Evidence has been presented to show how snow dynamics influence seasonal growth dynamics by influencing soil temperature in mountain forests. Soil temperature was the microclimate variable most relevant to the production of mature tracheids, highly influencing timing (onset and cessation) and resulting growth rates. As snowpack duration determines soil warming at the beginning of the growing season, a larger and more lasting snowpack induces a retarded cambial reactivation and is related to lower growth rates. Hence, this study at intra-annual scale, confirms what Sanmiguel-Vallelado et al. (2019) found at inter-annual scale in a tree-ring network of *P. uncinata* forests. The results provide additional information about the effects of climate and soil temperature and humidity conditions on radial growth.

The winter snow accumulation, the time of melt-out date, the onset of the growing season and the growth rates were strongly interrelated (Helama et al., 2013; Kirdyanov et al., 2003). In this study it was observed that larger snow accumulation involved later snow depletion that, in connection with lower spring air temperatures, produced a delay in soil warming onset and in tracheid maturation. Therefore, the most limiting factor to xylem development found in this study was low soil temperature in June. On the one hand, the soil cooling induced by snow presence can be explained by the effects of high snow albedo and high latent heat due to snowmelt is a heat sink (Zhang, 2005). On the other hand, low soil temperatures had been reported to inhibit root activity (Alvarez-Uria and Körner, 2007), which could explain an indirect effect on cambium reactivation in the spring, since roots provide water and nutrients to meristems such as the cambium. Several potential physiological mechanisms by which cool soils may limit conifer growth have been described in the literature. Kozlowski (1964) suggested that trees cannot uptake water through their roots and initiate hydraulic and metabolic processes until snowpacks wane to a threshold at which soil temperatures increase and viscosity decreases. CO<sub>2</sub> uptake was decreased at low root temperatures and appeared to be influenced by the pattern of nitrogen translocation (Vapaavuori et al., 1992). In cold substrates (< 5 °C), root growth in *P. sylvestris* has been found to be constrained by plasma membrane H<sup>+</sup>-ATPase (PM-ATPase) transport, which has multiple functions in cell growth (Iivonen et al., 1999). Furthermore, Peterson and Peterson (2001) suggest that increased cloudiness, associated with cool springs and late-lying snowpacks, could reduce solar radiation and increase the frequency of photo-inhibition following cold nights.

The highest correlation between air temperature and xylem development rates in most plots was found when the first radially enlarging tracheids were formed. By this time, the observed mean air temperature (6 °C) is similar to the 5 °C minimal air temperature threshold proposed by Rossi et al. (2008) for conifers from cold sites. Previous tree-ring studies demonstrated that low air temperatures during the growing

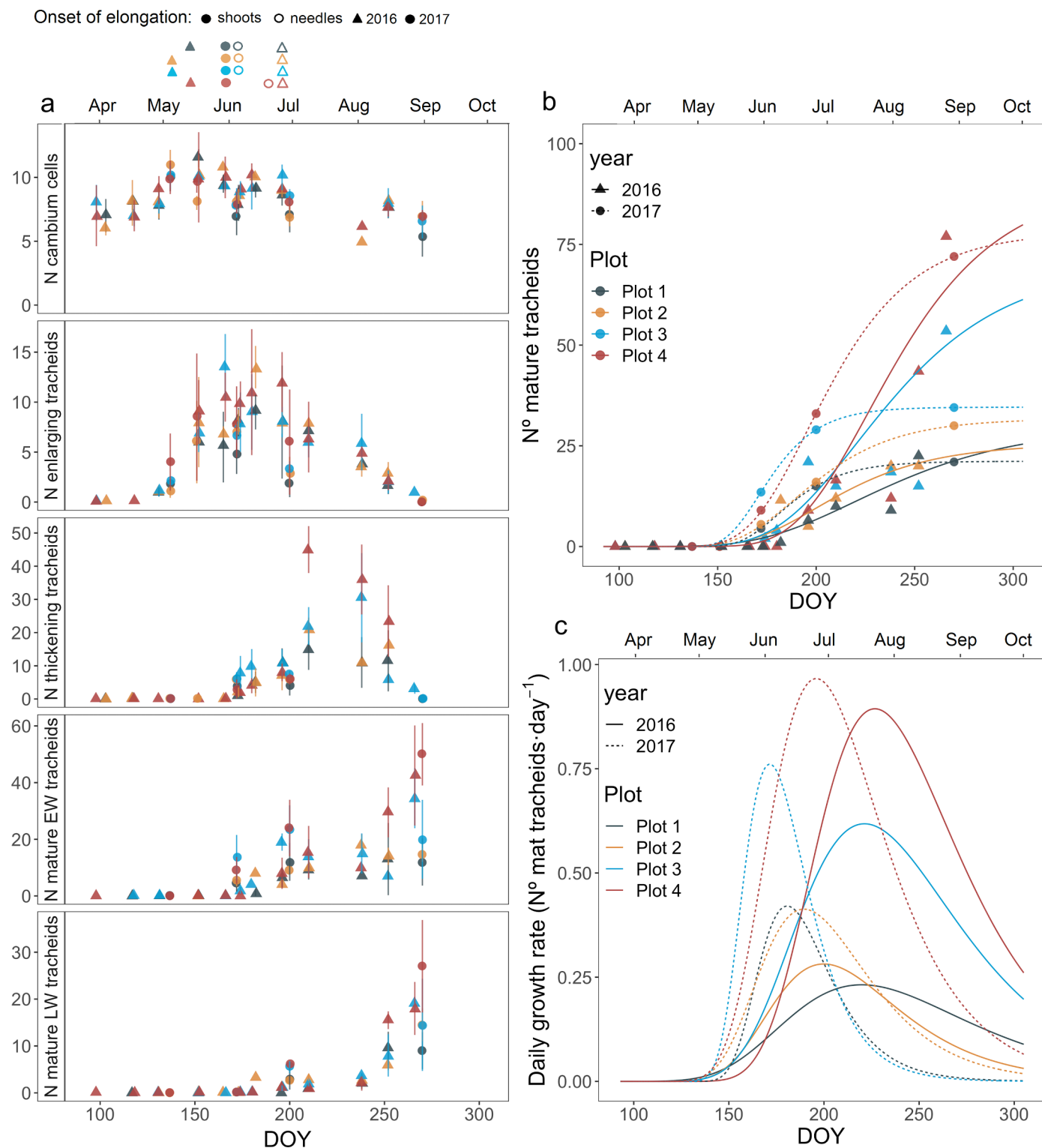


**Figure 3.** (a) Number of cambial cells and number of tracheids in the radial enlarging, wall-thickening and mature phases during 2016 and 2017. Median values by plot are shown. Bars represent inter-tree variability (standard deviation). Over the top of the plot the onset of shoot and needle elongation for each study plot and year are indicated. (b) Observed (dots) and Gompertz-modelled (lines) function of the number of mature tracheids during 2016 and 2017. (c) Estimated daily rates of production of mature tracheids by plot (daily number of produced mature tracheids) during 2016 and 2017. Timing is represented by the day of the natural year (DOY).

season limit growth of *P. uncinata* (Andreu et al., 2007; Camarero et al., 1998; Galván et al., 2014; Rolland and Schueller, 1994; Tardif et al., 2003). Nevertheless, due to the stronger coupling between mature tracheids and soil temperature observed in this study, we argue that 10°C soil temperature when first mature tracheids were developed

should be also considered.

Tracheid maturation onset always occurred after complete melt-out. In most cases, it was observed that a later tracheid maturation leads to a shorter growing season and, therefore, limits growth and wood production (Lenz et al., 2013). The observed reduction in growth rates

**Table 3**

Average needle and sapwood concentrations (%) as soluble sugars (SS), starch and total non-structural carbohydrates (TNC) during 2016.

	Plot	Needles				Sapwood			
		April	June	August	October	April	June	August	October
SS	1	5.6	6.7	5.4	4.8	0.7	0.7	0.6	1.4
	2	4.6	7.6	10.5	7.2	3.9	4.0	3.9	5.6
	3	10.2	14.2	15.8	12.0	4.6	4.7	4.6	6.9
	4	5.4	4.6	3.9	4.2	0.5	0.7	0.7	1.0
Starch	1	14.1	20.4	6.7	7.9	3.4	3.9	3.7	4.8
	2	19.5	25.0	10.6	12.1	3.9	4.6	4.4	5.8
	3	5.5	4.6	5.2	4.8	0.6	0.6	0.8	1.1
	4	8.9	5.4	9.9	4.9	3.0	3.5	3.4	4.3
TNC	1	14.3	10.0	15.2	9.7	3.6	4.1	4.2	5.5
	2	5.9	4.7	7.0	4.2	1.5	0.8	1.1	1.2
	3	9.3	6.9	5.5	6.4	4.3	4.7	4.4	5.2
	4	15.2	11.6	12.5	10.6	5.8	5.5	5.4	6.4

induced by snow-related cold soil temperatures is more relevant to wood production than growing season duration (Cuny et al., 2015). Apart from that, low soil temperatures in September reduced xylem development; therefore, the soil cooling in early autumn seems also to affect the last phases of xylogenesis (Cuny et al., 2014). These results agree with the negative influences that Sanmiguel-Vallelado et al. (2019) found between winter snow accumulation and late spring snow presence on *P. uncinata* growth and provide an in-depth explanation at a finer temporal resolution.

Although the highest NSC concentration in sapwood was found in the coldest plot, no difference in NSC concentration was found among plots along the altitudinal gradient, and there was no link with growth dynamics. Similarly, Gruber et al. (2011) did not find evidence that an insufficient carbon balance limits growth at their upper elevational limit. This confirms that radial growth and the storage and mobilization of carbon pools are not necessarily coupled (Körner, 2012). The needle starch concentration was observed when needles started elongating during June in some plots (e.g. plot 2), and this was followed by a peak in SS concentration in August, suggesting the differential use of these NSCs to build the new foliage. Since highest NSC concentration in sapwood occurred in October, when xylogenesis finished, the observed dynamics of sapwood NSC did not follow xylogenesis, whereas in other studies they were more coupled to latewood formation (Oberhuber et al., 2011).

The onset of stem radial increment in *P. uncinata* (DOY 130 ± 15), occurred on average 15 days in advance of the onset of mature tracheid formation, probably reflected the date when stem re-hydration started (Zweifel et al., 2000). We observed a value of 6 °C in 7-day average soil temperature for the onset of stem radial increment, which agrees with the fact that soil temperatures lower than 6 °C inhibit water uptake by roots in several conifers (Alvarez-Uria and Körner, 2007). As water from snow melting infiltrates into the soil during winter, it is available for trees even before the complete snow depletion, once the soil starts warming and triggers fine root activity. Warmer air temperatures in May – we observed a value of 8 °C in 7-day average air temperature for the onset of stem radial increment – promoted stem radial increment rates in the study area, may be because they facilitated water release from snow – we observed an important water contribution to soil moisture from snowmelt in that time – and stimulated cambium resumption (Camarero et al., 1998). Radial increment rates were mainly driven by soil moisture and air humidity, reflecting the strong linkage between stem radial fluctuations and changes in tree water status even in high-elevation forests (Zweifel et al., 2000). However, only a positive influence of early spring snowmelt on xylem development was observed in plot 1, where the lowest soil moisture values are found. Therefore, we cannot demonstrate that snowmelt water promoted *P. uncinata* growth in the study site. Similarly, Turcotte et al. (2009) reported that growth initiation in black spruce was not limited by the spring rehydration. This soil moisture limitation was reported in more arid mountain ranges (St. George, 2014). The cessation of the stem radial

increment period and the start of latewood formation are triggered by warm-dry air and soil conditions in summer.

We found no clear microclimate influences on maximum rates of production of mature tracheids or radial increment, neither in terms of timing nor in magnitude. It has been reported that the maximum growth rates of conifers from cold sites synchronized with the longest day in the year (Rossi et al., 2006). Our observations agree with this idea since stem radial maximum rates occurred around 10 days earlier than the summer solstice.

We also observed a high variability in small spatial scale in microclimate conditions and also in tree growth and NSCs. All plots showed similar snow influences on seasonal growth dynamics, with some variation in strength; however, when considering annual snow-growth effects and the inter-plot variability, plot 4 stepped out of line. This plot (the coldest site situated at highest elevation and with a northern aspect) showed the longest growing season and largest growth rates despite the presence of the longest-lasting snowpacks, contrary to what was expected. This behavior in plot 4 could be explained by high solar radiation values in spring. In addition, more water availability, and for longer periods, may prevent *P. uncinata* from drought, in contrast to what can occur when water is scarce during summer in shallow and rocky soils (Galván et al., 2014). However, more research will be needed to determine which ultimate factors determine the differences between plots. Therefore, *P. uncinata* growth was determined, to a large extent, by snow dynamics in 3 out of the 4 studied plots. Excepting plot 4, a later snow melt-out date delayed and shortened the *P. uncinata* growing season, thus reducing growth. Rossi et al. (2011) previously confirmed that delayed snowmelt reduced growth in boreal forests of *Picea mariana* in Quebec, Canada. Previously, Vaganov et al. (1999) found that in the Russian taiga conifers showed a lower growth when snow melt was delayed in the early growing season. This study extends these observations to high-elevation mountain forests of mid-latitude ranges such as the Pyrenees, and highlights the need to consider the small-scale variability of microclimate effects on individual tree growth of mountain forests.

The abovementioned inter-plot variability in microclimate conditions and tree growth was much larger than inter-annual variability in most cases. Inter-annual variability in growth dynamics may be induced by microclimate conditions, at least in a part. For example, in 2016, the warmest air and soil temperatures observed during the TGS might promote the highest production of mature tracheids. All our four sites are mainly characterized by temperature limitation of growth, as we have discussed previously. Therefore, low temperatures during the growing season limit the tree growth (Rossi et al., 2008). In 2017, the earliest melt-out dates might lead to the earliest starting and peaking date of mature tracheids production. We previously mentioned that the energy-limited influence of snow on studied forest, due to long-lasting snowpacks, could be an appropriate explanation for the positive influence of soil temperature on tree growth found in this study (Helama et al., 2013; Kirdyanov et al., 2003). In 2018, the highest

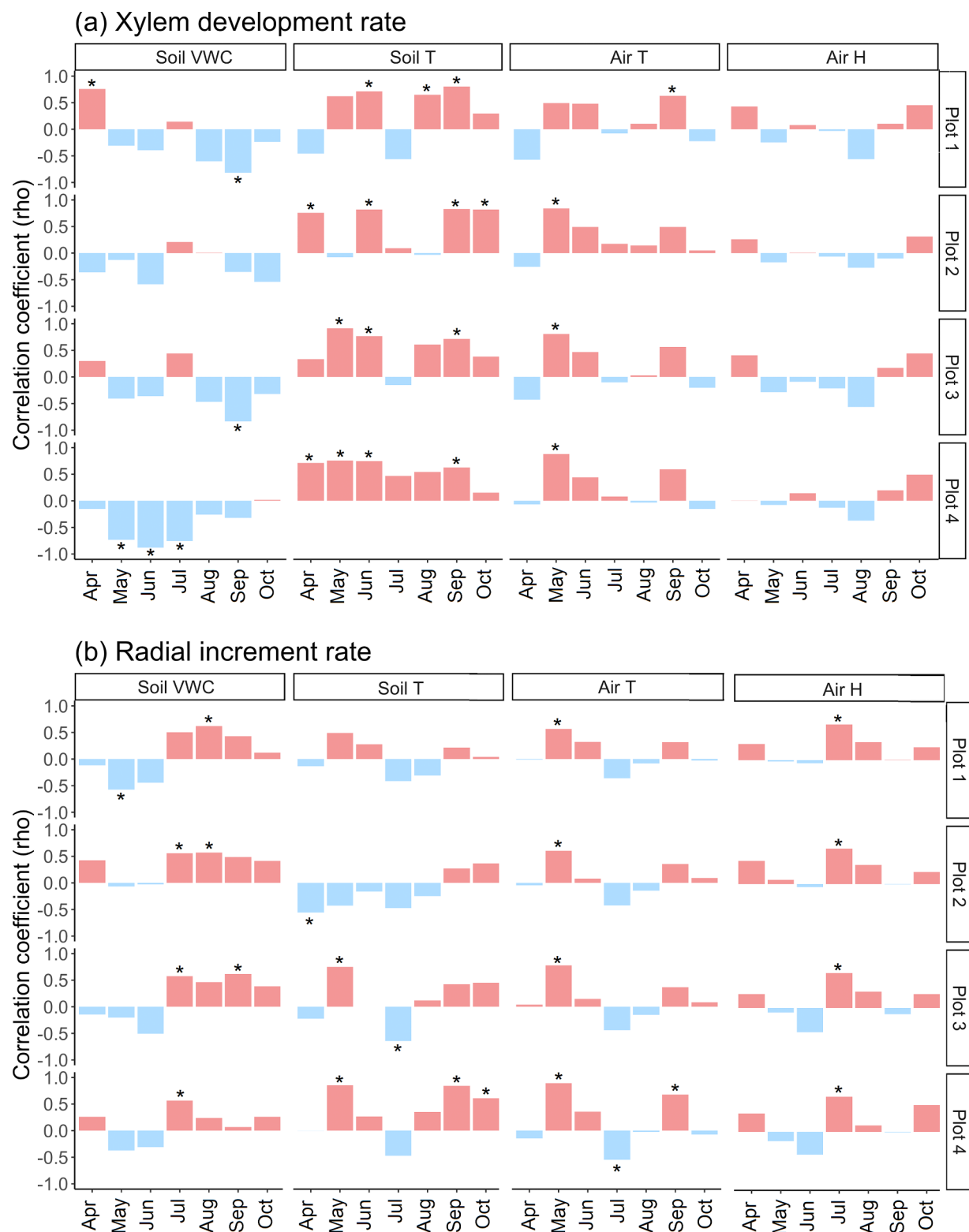


**Figure 4.** Spearman rho correlation coefficients calculated by month and plot between microclimate variables (weekly averages) and tree growth rates data series (weekly maximum values) of *P. uncinata* during the main growing period. (a) Xylem development rates corresponding to the production of mature tracheids comprised two years (2016, 2017) and (b) radial increment rates series comprised three years (2016, 2017, 2018). Therefore, the number of samples varied among correlations; as a consequence, critical values for Spearman coefficients varied too. Asterisks highlight significant correlations ( $p < 0.05$ ).

radial growth observed might reflect the largest soil moisture conditions during the growing season. As previously stated, we found evidence that stem radial fluctuations were strongly related to tree hydrous state in the studied forests (Zweifel et al., 2000). Under the

current climate warming context, increasing trends in air temperature had been already reported in the Spanish Pyrenees (El Kenawy et al., 2011). Future warmer air and soil temperatures are expected to prolong the *P. uncinata* growing season, and therefore, to enhance growth of

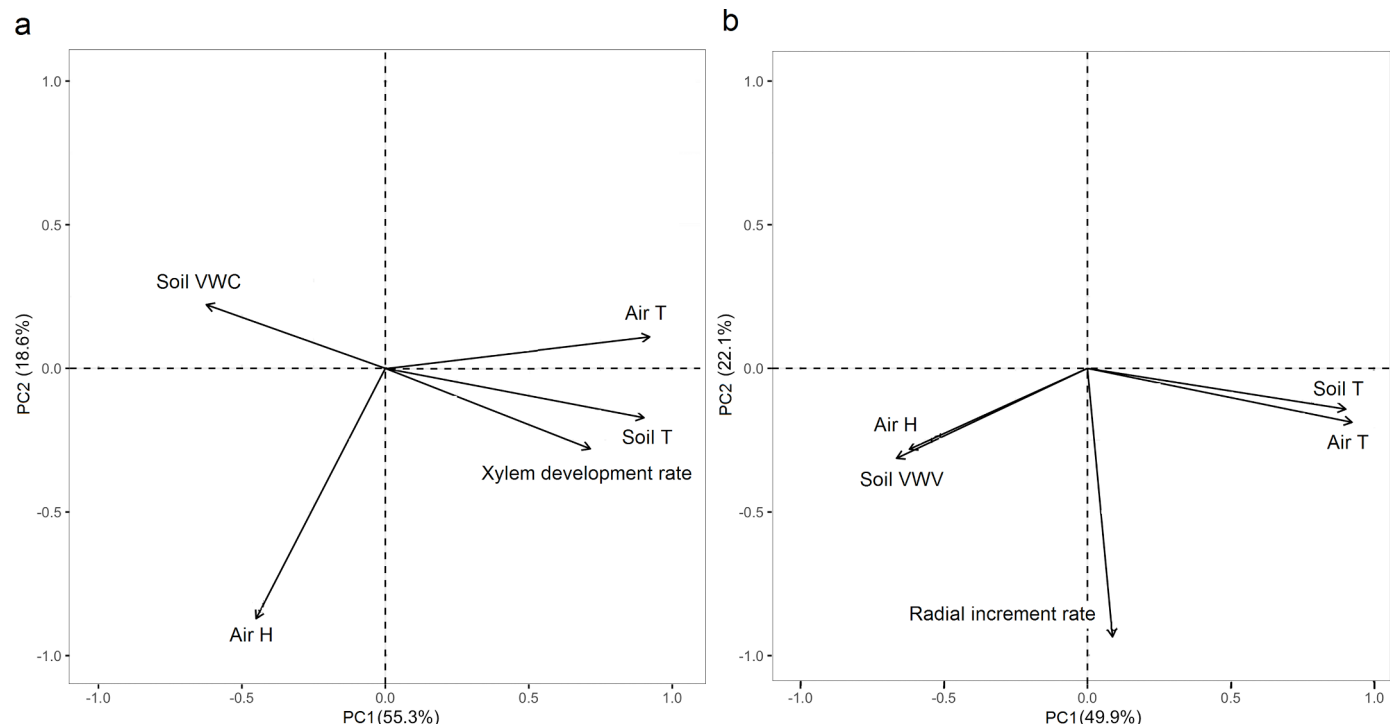


**Figure 5.** Principal component analysis of microclimate variables (weekly averages) and *P. uncinata* tree growth rates (weekly maximum values) during the main growing period. (a) Xylem development rates series corresponding to the production of mature tracheids comprised two years (2016, 2017) and (b) radial increment rates series comprised three years (2016, 2017 and 2018).

Pyrenean high-elevation forests and treelines during the late 21<sup>st</sup> century (Camarero et al., 2017; Sánchez-Salguero et al., 2012). An increase in precipitation variability has been also reported in this mountain range (López-Moreno et al., 2010). Therefore, these forecasts could be amplified if climate change also affects snow dynamics (accumulation, duration and melting) leading to shallower snowpacks and a longer snow-free period (Alonso-González et al., 2020; Morán-Tejeda et al., 2017; López-Moreno et al., 2017). Overall, growth of high-elevation *P. uncinata* novel forests could be benefited from the projected future snow and air temperature projections. This positive effect could be explained by a longer growing season, and a subsequently enhanced growth rate due to an earlier rise and a later cooling of soil temperatures. Faster growth rates are related to shorter tree longevity, and it is expected to lead to a reduced capacity of old forest ecosystems to store carbon under warmer future (Büntgen et al., 2019), but new young forests could also represent relevant carbon pools.

## 5. Conclusions

The seasonal growth dynamics of high-elevation *P. uncinata* forests were affected by snow dynamics. Soil temperature was the most relevant microclimate variable during the overall xylogenesis, mainly influencing the production of mature tracheids. Larger snow accumulation involved later snow depletion that produced a delay in soil warming onset. Low soil temperatures in spring, due to prolonged snow persistence, retarded the cambial onset and reduced growth rates. Wood production was affected by snow dynamics in three out of the four studied plots through a delayed and shorter growing season. This study highlights the large role of early and late growing season soil

temperatures on radial growth, in addition to the widely reported effect of air temperature. A future shallower and more ephemeral snowpack in similar mountain, young forests, together with warmer air and soil temperatures, may enhance productivity and tree growth by prolonging the growing season through an earlier onset and a late cessation of xylogenesis.

## Declaration of Competing Interest

The authors declare that they have no known competing financial interests or personal relationships that could have appeared to influence the work reported in this paper.

## Acknowledgements

We sincerely thank colleagues, friends and relatives who helped during the field surveys. This study was supported by the projects: “*Bosque, nieve y recursos hídricos en el Pirineo ante el cambio global*” funded by Fundación Iberdrola, CGL2014-52599-P (IBERNIEVE) and CGL2017-82216-R (HIDROIBERNIEVE) funded by the Spanish Ministry of Economy and Competitiveness. ASV was supported by a pre-doctoral University Professor Training grant [FPU16/00902] funded by the Spanish Ministry of Education, Culture and Sports. EAG was supported by a pre-doctoral FPI grant [BES-2015-071466] funded by the Spanish Ministry of Economy and Competitiveness. JJC, AG and MC acknowledge funding by project RTI2018-096884-B-C31 (Spanish Ministry of Economy and Competitiveness).

## Appendix

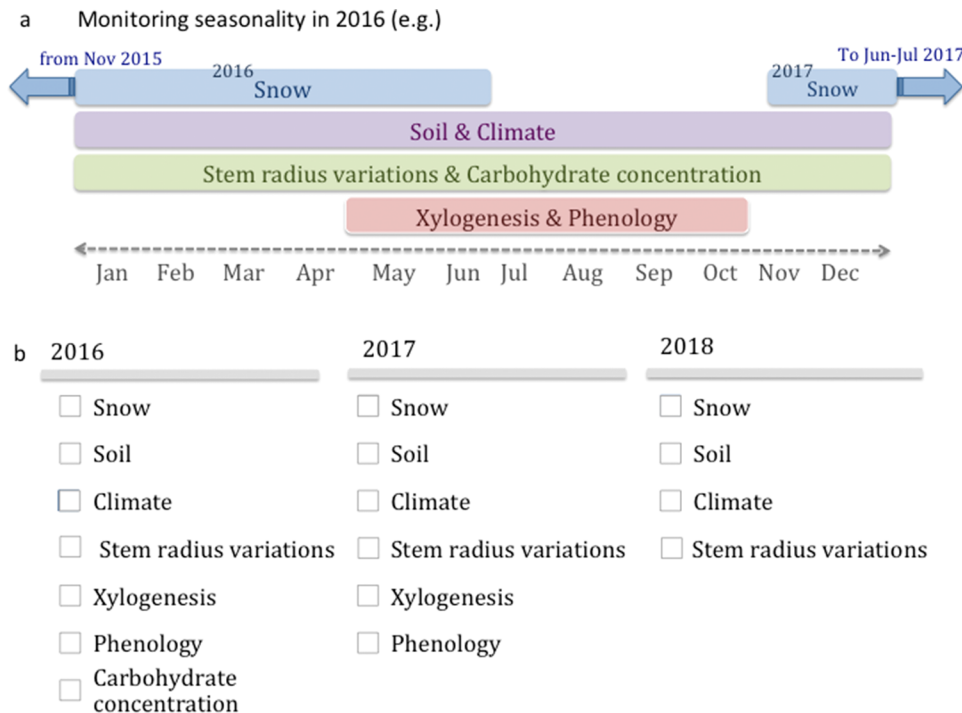


Figure A.1. (a) Monitoring seasonality throughout 2016 as an example of one year of data collection, and (b) differences in variables acquired among years.

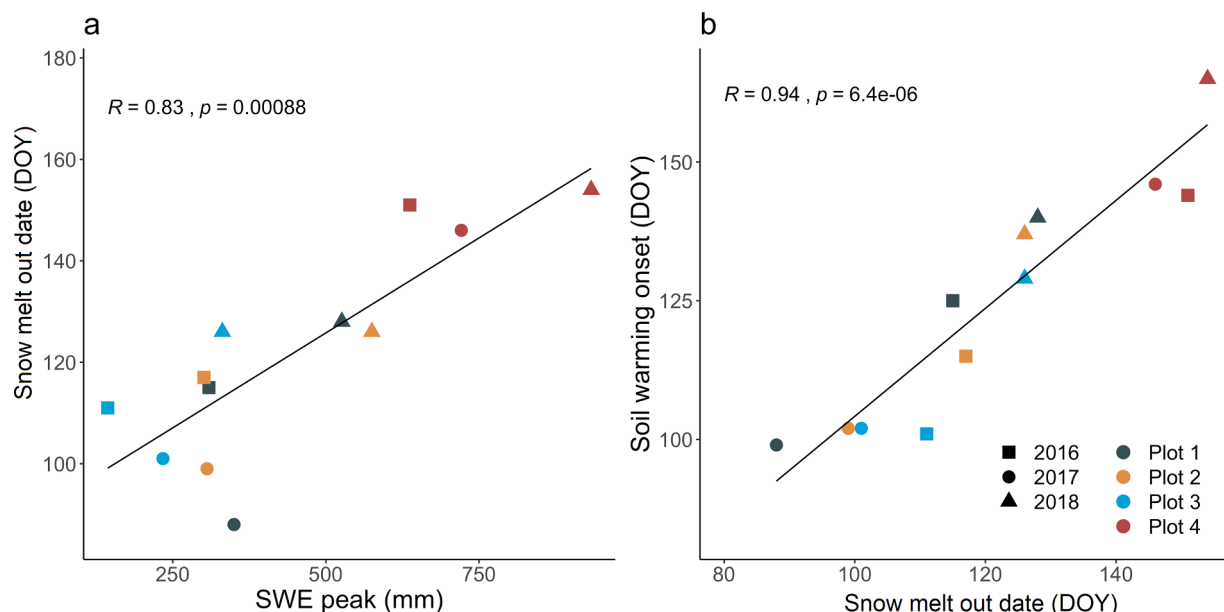
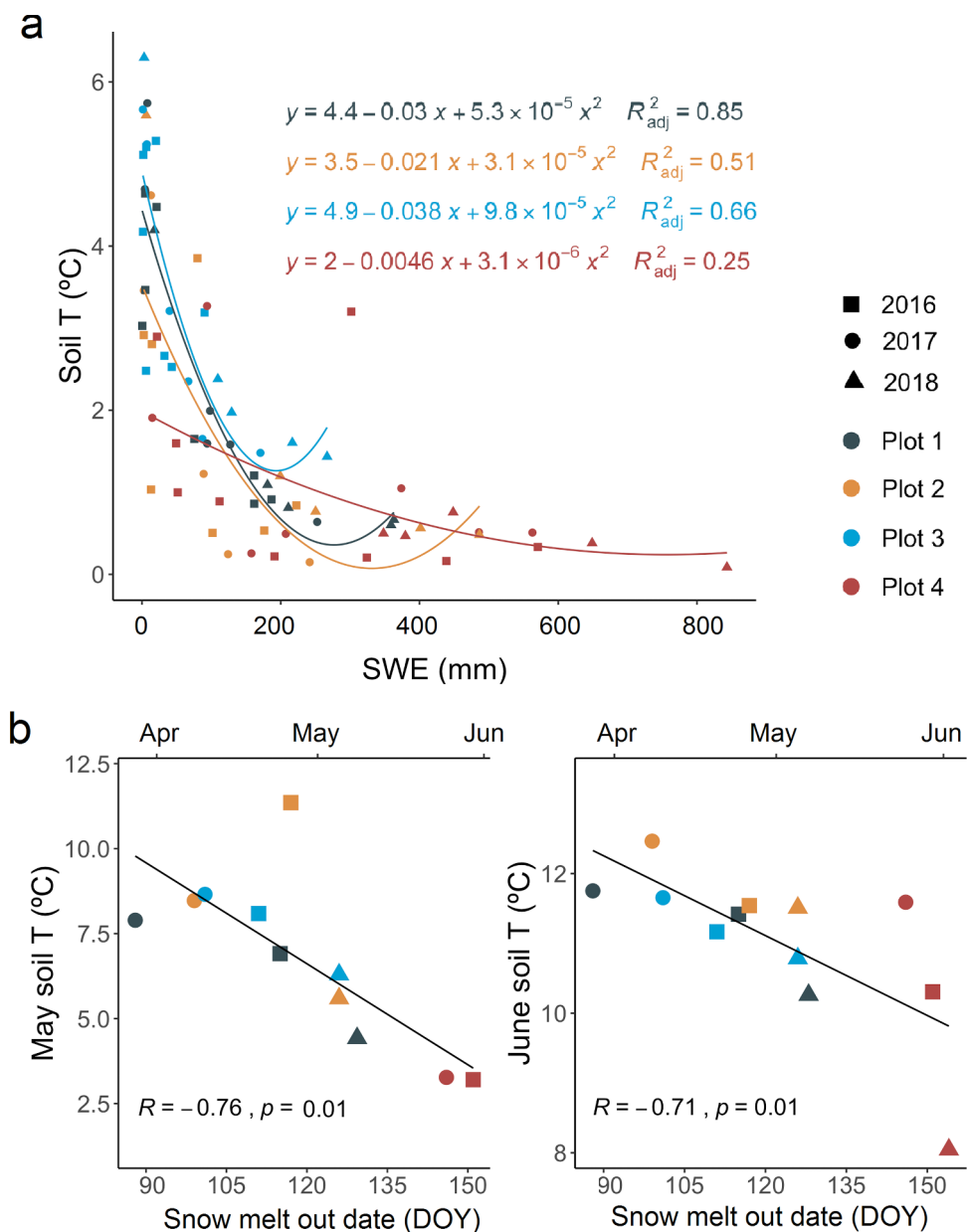
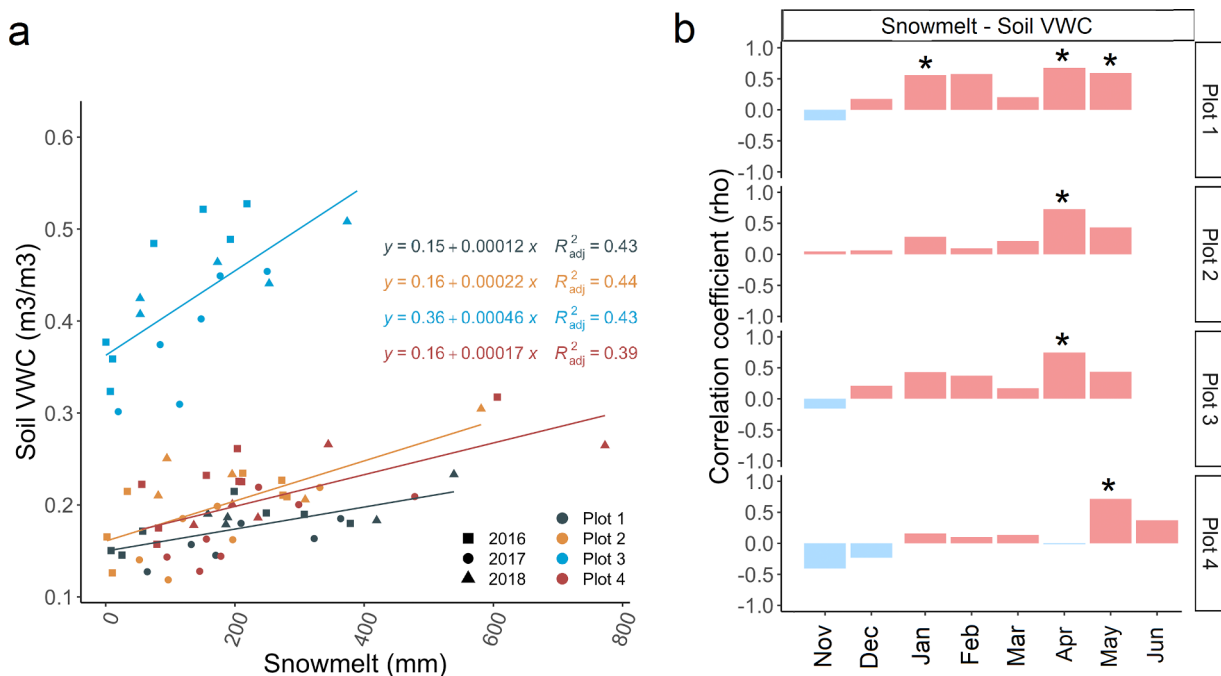


Figure A.2. Scatterplot of the relationships between (a) SWE peak and snowmelt out date and (b) between snow melt out date and soil warming onset. Pearson correlation coefficients between indices and  $p$  values are shown.



**Figure A.3.** (a) Polynomial regressions between monthly averages of SWE and soil temperature by plot for the four study plots considering data collected during 2016, 2017 and 2018. (b) Scatterplots of timing of melt-out date and May and June soil temperatures considering data collected during 2016, 2017 and 2018. Pearson correlation coefficients and  $p$  values are shown.



**Figure A.4.** (a) Linear regressions between monthly sums of snowmelt and monthly averages of soil VWC by plot considering data collected during 2016, 2017 and 2018 (b) Spearman correlation coefficients calculated by month and plot between snowmelt weekly sums and soil VWC weekly averages considering data collected during 2016, 2017 and 2018. Asterisks highlight significant correlations ( $p < 0.05$ ). Note that the number of samples and significance levels varied among months and plots.

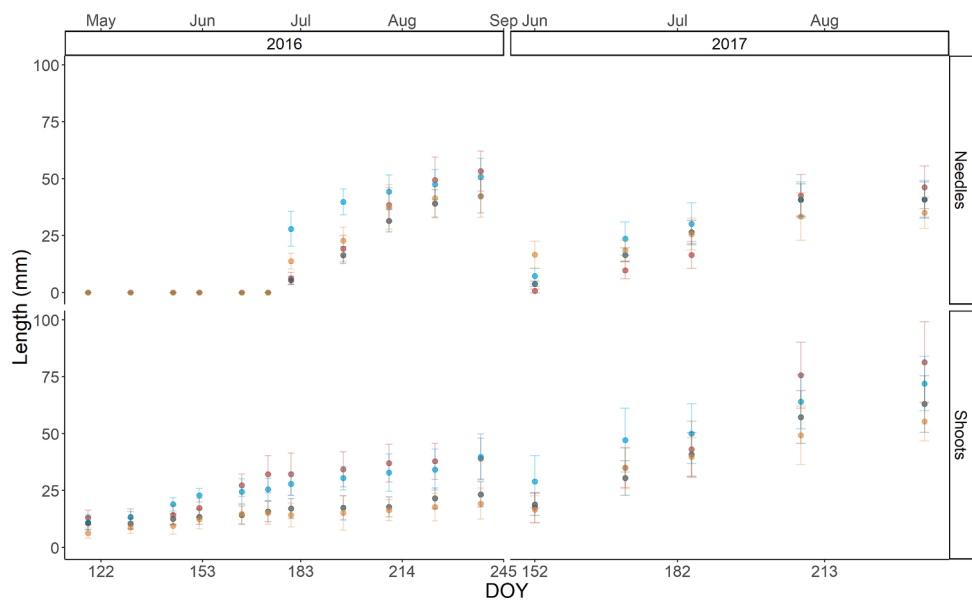


**Figure A.5.** Time series of needle (top panel) and shoot (bottom panel) length during the 2016 and 2017 growing seasons (dots: mean values; error bars: standard deviation). Timing is represented by the day of the natural year (DOY).

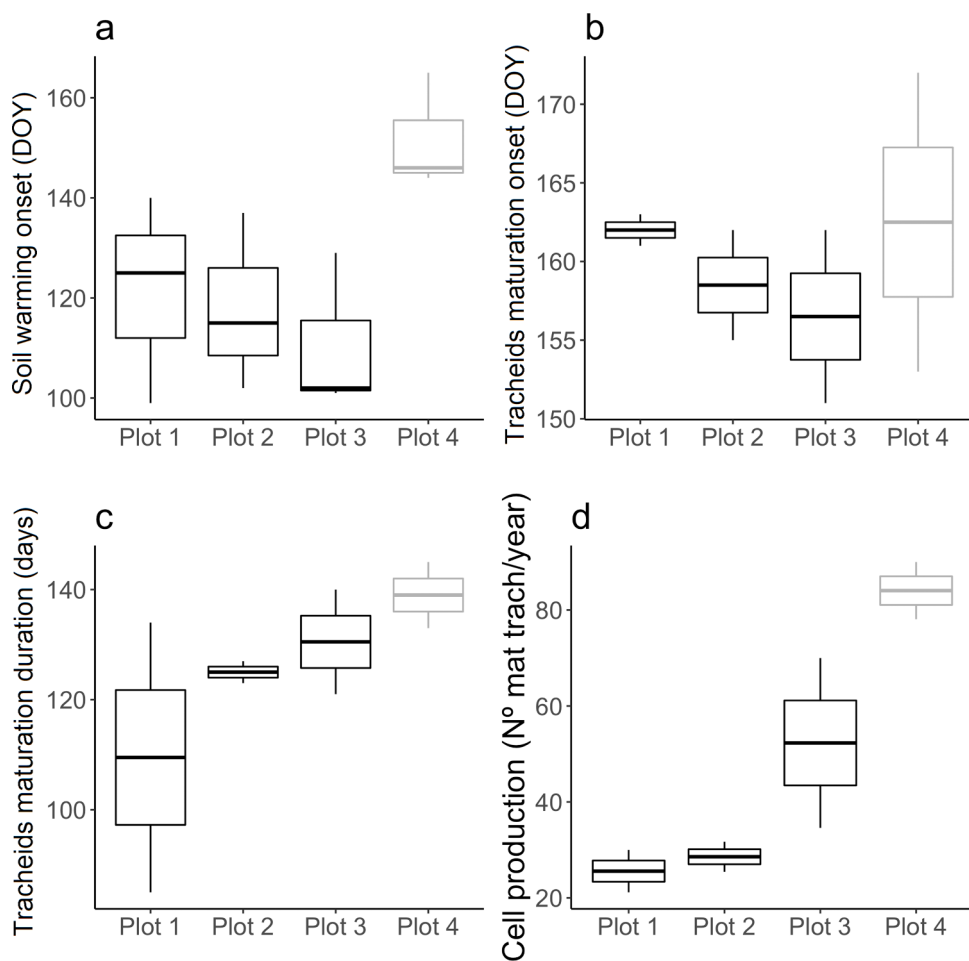


**Figure A.6.** Boxplots of related soil temperature and xylogenesis variables: (a) soil warming onset, (b) tracheid maturation onset, (c) tracheid maturation duration and (d) rate of production of mature tracheids. In grey, plot 4 was highlighted since it presented “outlier” microclimate conditions and growth characteristics.

**Table A.1**  
Descriptive indices calculated from tree growth data.

	Index	Description
Stem radial increment	Total stem radial increment	Parameter A of Gompertz function adjusted to daily maximum radius series (upper asymptote).
	Stem radial increment onset	Date when daily rates of radial increment exceeded $3 \mu\text{m} \cdot \text{day}^{-1}$ .
	Stem radial increment cessation	Date when daily rates of radial increment fell below $3 \mu\text{m} \cdot \text{day}^{-1}$ .
	Stem radial increment duration	Time between the onset and cessation dates of stem radial increment.
	Maximum rate of radial increment	Maximum value obtained from estimated daily rates of radial increment series.
Mature tracheids	Timing of maximum rate of radial increment	Date when maximum rate of radial increment was reached.
	Production of mature tracheids	Parameter A of Gompertz function adjusted to mature cell number increase series (upper asymptote); i.e. number of mature tracheids developed per year.
	Maturation onset	Date when first mature tracheid was completely developed, obtained from Gompertz function adjusted to mature cell number increase series.
	Maturation cessation	Date when last mature tracheid was completely developed, obtained from Gompertz function adjusted to mature cell number increase series.
	Maturation duration	Time between the onset and cessation dates of tracheid maturation.
Shoot and needle phenology	Maximum rate of mature tracheid development	Maximum value obtained from estimated daily rates of mature tracheid development series.
	Timing of maximum rate of mature tracheid development	Date when maximum rate of mature tracheid development was reached.
	Onset of shoot elongation	First day when an increment in shoot length was recorded after dormancy.
	Shoots final length	Maximum shoot length recorded.
	Onset of needle elongation	First day when an increment in needle length was recorded after dormancy.
	Needle final length	Maximum needle length value recorded.

**Table A.2**  
Average microclimate conditions during each year at each plot.

Year	Plot	Snowpack <sup>‡</sup>	Melt out date (DOY)	Duration (days)	SWE peak (mm)	Day of peak (DOY)	VWC peak (m <sup>3</sup> ·m <sup>-3</sup> )	Day of peak <sup>†</sup> (DOY)	VWC during TGS (m <sup>3</sup> ·m <sup>-3</sup> )	Min VWC (m <sup>3</sup> ·m <sup>-3</sup> )	Day of VWC min (DOY)	VWC (DOY)	Air			Duration of TGS (days)	T during TGS (°C)	Cooling (DOY)	H during TGS (%)	
													Soil Infiltr. onset (DOY)	VWC peak (m <sup>3</sup> ·m <sup>-3</sup> )	TGS (°C)	Warming (DOY)	T during TGS (DOY)	Duration of TGS (days)		
2016	1	2	115	114	309	47	7	0.24	130	0.10	0.01	252	125	11.7	311	125	184	11.6	309	63.6
	2	347	117	137	301	80	350	0.29	130	0.14	0.04	252	115	12.2	311	108	201	11.5	309	62.7
	3	2	111	110	144	75	3	0.58	91	0.24	0.06	252	107	10.9	326	107	202	12.5	309	62.4
	4	347	151	171	637	104	350	0.41	130	0.15	0.03	252	144	11.2	286	138	147	11.7	285	60.3
2017	1	2	88	86	350	45	11	0.21	132	0.12	0.05	235	98	9.3	312	68	240	10.4	308	62.4
	2	328	99	137	306	37	339	0.27	132	0.15	0.08	235	101	9.6	310	68	240	11.0	308	61.6
	3	11	101	90	234	38	14	0.50	133	0.29	0.08	291	101	9.5	330	67	241	11.7	308	61.2
	4	319	146	193	721	85	322	0.28	132	0.15	0.05	235	145	7.7	293	70	238	9.2	308	60.8
2018	1	336	128	158	526	101	348	0.28	99	0.14	0.05	248	139	9.9	308	109	191	11.1	300	72.1
	2	336	126	156	331	91	342	0.37	98	0.18	0.08	218	136	10.9	308	107	193	11.8	300	71.2
	3	336	126	156	331	102	329	0.34	129	0.17	0.06	219	164	9.0	300	110	189	12.4	300	71.4
	4	310	154	210	933													299	10.0	299

Abbreviations: Accum.: Accumulation; SWE: Snow Water Equivalent; Infilt.: Infiltration, VWC: Volumetric water content, Min: minimum, T: temperature; TGS: Thermal growing season; H: humidity

(‡) To calculate snow indices, snow seasons temporality was taken into account, not natural years (see Figure A.1).

(†) The first peaks of soil moisture at plot 1, plot 2 and plot 3 during 2017 snow season were not considered because they preceded snow accumulation (explained by an extraordinary precipitation event in November 2017, see Figure A.3), thus the second peak was shown here and used in analysis.

**Table A.3**

Variance accounted for (%) the two first principal components (PC1 and PC2) and correlations between them and original variables (weekly average microclimate conditions and weekly maximum growth rates). Values in bold indicate the two variables which contributed the most to each PC.

Variable	PCA 1: mature tracheid production	PCA 2: stem radial increment
	PC1 (55.3%)	PC1 (49.9%)
Soil T	0.54	0.57
Soil VWC	-0.38	-0.42
Air T	0.55	0.58
Air H	-0.27	-0.39
Daily growth rate	0.43	0.06
	PC2 (18.6%)	PC2 (22.1%)
	-0.18	-0.14
	0.23	-0.29
	0.11	-0.18
	-0.90	-0.27
	-0.29	-0.89

## References

- Albrich, K., Rammer, W., Seidl, R., 2020. Climate change causes critical transitions and irreversible alterations of mountain forests. *Glob. Change Biol.* <https://doi.org/10.1111/gcb.15118>.
- Alonso-González, E., López-Moreno, J.I., Navarro-Serrano, F., Sanmiguel-Vallelado, A., Aznárez-Balta, M., Revuelto, J., Ceballos, A., 2020. Snowpack Sensitivity to Temperature, Precipitation, and Solar Radiation Variability over an Elevation Gradient in the Iberian Mountains. *Atmos. Res.* 243, 104973. <https://doi.org/10.1016/j.atmosres.2020.104973>.
- Alvarez-Uria, P., Körner, C., 2007. Low temperature limits of root growth in deciduous and evergreen temperate tree species. *Funct. Ecol.* 21, 211–218. <https://doi.org/10.1111/j.1365-2435.2007.01231.x>.
- Andreu, L., Gutiérrez, E., Macias, M., Ribas, M., Bosch, O., Camarero, J.J., 2007. Climate increases regional tree-growth variability in Iberian pine forests. *Glob. Change Biol.* 13, 804–815.
- Antonova, G.F., Stasova, V.V., 1993. Effects of environmental factors on wood formation in Scots pine stems. *Trees* 7 (4), 214–219. <https://doi.org/10.1007/BF00202076>.
- Babst, F., Bouriaud, O., Poulet, B., Trouet, V., Girardin, M.P., Frank, D.C., 2019. Twentieth century redistribution in climatic drivers of global tree growth. *Sci. Adv.* 5 eaat4313.
- Barnett, T.P., Adam, J.C., Lettenmaier, D.P., 2005. Potential impacts of a warming climate on water availability in snow-dominated regions. *Nature* 438 (7066), 303–309. <https://doi.org/10.1038/nature04141>.
- Beniston, M., 2012. Is snow in the Alps receding or disappearing? *Wiley Interdiscip. Rev. Clim. Change* 3, 349–358.
- Breiman, L., 2001. Random forests. *Mach. Learn* 45, 5–32.
- Büntgen, U., Krusic, P.J., Piermattei, A., Coomes, D.A., Esper, J., Myglan, V.S., Kirdyanov, A.V., Camarero, J.J., Crivellaro, A., Körner, C., 2019. Limited capacity of tree growth to mitigate the global greenhouse effect under predicted warming. *Nat. Commun.* 10, 2171. <https://doi.org/10.1038/s41467-019-10174-4>.
- Camarero, J.J., Guerrero-Campo, J., Gutiérrez, E., 1998. Tree-Ring Growth and Structure of *Pinus uncinata* and *Pinus sylvestris* in the Central Spanish Pyrenees. *Arct. Alp. Res.* 30, 1. <https://doi.org/10.2307/1551739>.
- Camarero, J.J., Linares, J.C., García-Cervigón, A.I., Batllori, E., Martínez, I., Gutiérrez, E., 2017. Back to the future: the responses of alpine treelines to climate warming are constrained by the current ecotone structure. *Ecosystems* 20, 683–700.
- Camarero, J.J., Olano, J.M., Parras, A., 2010. Plastic bimodal xylogenesis in conifers from continental Mediterranean climates. *New Phytol* 185, 471–480. <https://doi.org/10.1111/j.1469-8137.2009.03073.x>.
- Cantegrel, R., 1983. Le Pin à crochets pyrénéen: biologie, biochimie, sylviculture. *Acta Biol. Mont.* 2, 87–330.
- Carlson, K.M., Coulthard, B., Starzomski, B.M., 2017. Autumn snowfall controls the annual radial growth of centenarian whitebark pine (*Pinus albicaulis*) in the southern Coast Mountains, British Columbia, Canada. *Arct. Antarct. Alp. Res.* 49, 101–113.
- Cuny, H.E., Rathgeber, C.B.K., Frank, D., Fonti, P., Fournier, M., 2014. Kinetics of tracheid development explain conifer tree-ring structure. *New Phytol* 203, 1231–1241. <https://doi.org/10.1111/nph.12871>.
- Cuny, H.E., Rathgeber, C.B.K., Frank, D., Fonti, P., Mäkinen, H., Prislan, P., Rossi, S., del Castillo, E.M., Campelo, F., Vavrčík, H., Camarero, J.J., Bryukhanova, M.V., Jyske, T., Gričar, J., Gryc, V., De Luis, M., Vieira, J., Čufar, K., Kirdyanov, A.V., Oberhuber, W., Tremel, V., Huang, J.-G., Li, X., Swidrak, I., Deslauriers, A., Liang, E., Nöjd, P., Gruber, A., Nabais, C., Morin, H., Krause, C., King, G., Fournier, M., 2015. Woody biomass production lags stem-girth increase by over one month in coniferous forests. *Nature Plants* 1, 15160. <https://doi.org/10.1038/nplants.2015.160>.
- D'Orangeville, L., Côté, B., Houle, D., Morin, H., Duchesne, L., 2013. A three-year increase in soil temperature and atmospheric N deposition has minor effects on the xylogenesis of mature balsam fir. *Trees* 27, 1525–1536. <https://doi.org/10.1007/s00468-013-0899-4>.
- Dan Moore, R., Spittlehouse, D., Story, A., 2005. Riparian microclimate and stream temperature response to forest harvesting: a review. *Am. Water Resour. Assoc.* 41, 813–834.
- Del Barrio, G., Creus, J., Puigdefábregas, J., 1990. Thermal seasonality of the high mountain belts of the Pyrenees. *Mt. Res. Dev.* 227–233.
- Denne, M.P., 1989. Definition of Latewood According to Mork (1928). *Am. Water Resour. Assoc.* 10, 59–62. <https://doi.org/10.1163/22941932-90001112>.
- Deslauriers, A., Rossi, S., Anfodillo, T., 2007. Dendrometer and intra-annual tree growth: What kind of information can be inferred? *Dendrochronologia* 25, 113–124. <https://doi.org/10.1016/j.dendro.2007.05.003>.
- Deslauriers, A., Rossi, S., Liang, E., 2015. Collecting and Processing Wood Microcores for Monitoring Xylogenesis, in: Yeung, E.C.T., Stasolla, C., Sumner, M.J., Huang, B.Q. (Eds.), *Plant Microtechniques and Protocols*. Springer International Publishing, Cham, pp. 417–429. [https://doi.org/10.1007/978-3-319-19944-3\\_23](https://doi.org/10.1007/978-3-319-19944-3_23).
- El Kenawy, A., López-Moreno, J.I., Vicente-Serrano, S.M., 2011. Recent trends in daily temperature extremes over northeastern Spain (1960–2006). *Nat. Hazards Earth Syst. Sci.* 11, 2583–2603. <https://doi.org/10.5194/nhess-11-2583-2011>.
- Galván, J.D., Camarero, J.J., Gutiérrez, E., 2014. Seeing the trees for the forest: drivers of individual growth responses to climate in *Pinus uncinata* mountain forests. *J. Ecol.* 102, 1244–1257.
- Gruber, A., Pirkebner, D., Oberhuber, W., Wieser, G., 2011. Spatial and seasonal variations in mobile carbohydrates in *Pinus cembra* in the timberline ecotone of the Central Austrian Alps. *Eur. J. For. Res.* 130, 173–179. <https://doi.org/10.1007/s10342-010-0419-7>.
- Harpold, A.A., Molotch, N.P., Musselman, K.N., Bales, R.C., Kirchner, P.B., Litvak, M., Brooks, P.D., 2015. Soil moisture response to snowmelt timing in mixed-conifer subalpine forests. *Hydrolog. Process.* 29, 2782–2798. <https://doi.org/10.1002/hyp.10400>.
- Helama, S., Mielikainen, K., Timonen, M., Herva, H., Tuomenvirta, H., Venalainen, A., 2013. Regional climatic signals in Scots pine growth with insights into snow and soil associations. *Dendrobiology* 70.
- Iivonen, S., Rikala, R., Ryypä, A., Vapaavuori, E., 1999. Responses of Scots pine (*Pinus sylvestris*) seedlings grown in different nutrient regimes to changing root zone temperature in spring. *Tree Physiology* 19, 951–958.
- Jolliffe, I.T., 2002. Choosing a Subset of principal Components or Variables. Principal Component Analysis. Springer Series in Statistics. Springer, New York, NY [https://doi.org/10.1007/0-387-22440-8\\_6](https://doi.org/10.1007/0-387-22440-8_6).
- Kaiser, H.F., 1974. An index of factorial simplicity. *Psychometrika* 39, 31–36.
- Kirdyanov, A., Hughes, M., Vaganov, E., Schweingruber, F., Silkin, P., 2003. The importance of early summer temperature and date of snow melt for tree growth in the Siberian Subarctic. *Trees* 17, 61–69.
- Körner, C., 2012. Alpine treelines: functional ecology of the global high elevation tree limits. Springer Science & Business Media.
- Kozłowski, T.T., 1964. *Water Metabolism in Plants*. Springer Series in Statistics. Springer, New York, NY [https://doi.org/10.1007/0-387-22440-8\\_6](https://doi.org/10.1007/0-387-22440-8_6).
- Lenz, A., Hoch, G., Körner, C., 2013. Early season temperature controls cambial activity and total tree ring width at the alpine treeline. *Plant Ecol. Divers.* 6, 365–375. <https://doi.org/10.1080/17550874.2012.711864>.
- López-Moreno, J.I., Gasco, S., Herrero, J., Sproles, E.A., Pons, M., Alonso-González, E., Hanich, L., Boudhar, A., Musselman, K.N., Molotch, N.P., Sickman, J., Pomery, J., 2017. Different sensitivities of snowpacks to warming in Mediterranean climate mountain areas. *Environ. Res. Lett.* 12 (7), 074006.
- López-Moreno, J.I., Vicente-Serrano, S.M., Angulo-Martínez, M., Beguería, S., Kenawy, A., 2010. Trends in daily precipitation on the northeastern Iberian Peninsula, 1955–2006. *Int. J. Climatol.* 30, 1026–1041.
- Lupi, C., Morin, H., Deslauriers, A., Rossi, S., 2012. Xylogenesis in black spruce: does soil temperature matter? *Tree Physiol.* 32, 74–82. <https://doi.org/10.1093/treephys/tpr132>.
- McCabe, G.J., Wolock, D.M., 2009. Recent declines in western US snowpack in the context of twentieth-century climate variability. *Earth Interact.* 13, 1–15.
- Morán-Tejeda, E., López-Moreno, J.I., Sanmiguel-Vallelado, A., 2017. Changes in climate, snow and water resources in the Spanish Pyrenees: observations and projections in a warming climate, in: *High Mountain Conservation in a Changing World*. Springer, pp. 305–323.
- Oberhuber, W., Swidrak, I., Pirkebner, D., Gruber, A., 2011. Temporal dynamics of non-structural carbohydrates and xylem growth in *Pinus sylvestris* exposed to drought. *Can. J. For. Res.* 41, 1590–1597. <https://doi.org/10.1139/x11-085>.
- Palacio, S., Maestro, M., Montserrat-Martí, G., 2007. Seasonal dynamics of non-structural carbohydrates in two species of mediterranean sub-shrubs with different leaf phenology. *Env. Exp. Bot.* 59, 34–42. <https://doi.org/10.1016/j.envexpbot.2005.10.003>.
- Pederson, G.T., Gray, S.T., Woodhouse, C.A., Betancourt, J.L., Fagre, D.B., Littell, J.S., Watson, E., Luckman, B.H., Graumlich, L.J., 2011. The unusual nature of recent snowpack declines in the North American Cordillera. *Science* 333, 332–335. <https://doi.org/10.1126/science.1201570>.
- Peterson, D.W., Peterson, D.L., 2001. Mountain Hemlock Growth Responds to Climatic Variability at Annual and Decadal Time Scales. *Ecology* 82, 3330–3345 [https://doi.org/10.1890/0012-9658\(2001\)082\[3330:MHGTC\]2.0.CO;2](https://doi.org/10.1890/0012-9658(2001)082[3330:MHGTC]2.0.CO;2).
- Core Team, R., 2018. *R Foundation for Statistical Computing*; Vienna, Austria: 2015. *R Lang. Environ. Stat. Comput.* 2013.
- Rasband, W.S., 1997. ImageJ. US National Institutes of Health, Bethesda, MD, USA. <http://rsb.info.nih.gov/ij/>.

- Rodríguez Pérez, D., 2013. Growthmodels: Nonlinear Growth Models. R package version 1.2.0. <https://CRAN.R-project.org/package=growthmodels>.
- Rolland, C., Schueler, J.F., 1994. Relationships between mountain pine and climate in the French Pyrenees (Font-Romeu) studied using the radiodensitometrical method. *Pirineos* 143, 55–70.
- Rossi, S., Deslauriers, A., Anfodillo, T., Carraro, V., 2007. Evidence of threshold temperatures for xylogenesis in conifers at high altitudes. *Oecologia* 152, 1–12. <https://doi.org/10.1007/s00442-006-0625-7>.
- Rossi, S., Deslauriers, A., Anfodillo, T., Morin, H., Saracino, A., Motta, R., Borghetti, M., 2006. Conifers in cold environments synchronize maximum growth rate of tree-ring formation with day length. *New Phytol* 170, 301–310. <https://doi.org/10.1111/j.1469-8137.2006.01660.x>.
- Rossi, S., Deslauriers, A., Gričar, J., Seo, J.W., Rathgeber, C.B., Anfodillo, T., Morin, H., Levanic, T., Oven, P., Jalkanen, R., 2008. Critical temperatures for xylogenesis in conifers of cold climates. *Glob. Ecol. Biogeogr.* 17, 696–707. <https://doi.org/10.1111/j.1466-8238.2008.00417.x>.
- Rossi, S., Deslauriers, A., Morin, H., 2003. Application of the Gompertz equation for the study of xylem cell development. *Dendrochronologia* 21, 33–39. <https://doi.org/10.1078/1125-7865-00034>.
- Rossi, S., Morin, H., Deslauriers, A., 2011. Multi-scale Influence of snowmelt on xylogenesis of Black Spruce. *Arct. Antarct. Alp. Res.* 43, 457–464. <https://doi.org/10.1657/1938-4246-43.3.457>.
- Rossi, S., Rathgeber, C.B.K., Deslauriers, A., 2009. Comparing needle and shoot phenology with xylem development on three conifer species in Italy. *Ann. For. Sci.* 66, 206. <https://doi.org/10.1051/forest/2008088>.
- Ruiz de la Torre, J., Ceballos, L., 1979. Arboles y Arbustos de la España Peninsular. ETSI de Montes, Madrid, pp. 512 ISBN 84-600-84-600.
- Sánchez-Salguero, R., Navarro-Cerrillo, R.M., Swetnam, T.W., Zavala, M.A., 2012. Is drought the main decline factor at the rear edge of Europe? The case of southern Iberian pine plantations. *For. Ecol. Manag.* 271, 158–169.
- Sangüesa-Barreda, G., Linares, J.C., Camarero, J.J., 2012. Mistletoe effects on Scots pine decline following drought events: insights from within-tree spatial patterns, growth and carbohydrates. *Tree Physiol* 32, 585–598. <https://doi.org/10.1093/treephys/tps031>.
- Sanmiguel-Vallelado, A., Camarero, J.J., Gazol, A., Morán-Tejeda, E., Sangüesa-Barreda, G., Alonso-González, E., Gutiérrez, E., Alla, A.Q., Galván, J.D., López-Moreno, J.I., 2019. Detecting snow-related signals in radial growth of *Pinus uncinata* mountain forests. *Dendrochronologia* 57, 125622. <https://doi.org/10.1016/j.dendro.2019.125622>.
- Sanmiguel-Vallelado, A., López-Moreno, J.I., Morán-Tejeda, E., Alonso-González, E., Navarro-Serrano, F.M., Rico, I., Camarero, J.J., 2020. Variable effects of forest canopies on snow processes in a valley of the central Spanish Pyrenees. *Hydrol. Process. Hyp* 13721. <https://doi.org/10.1002/hyp.13721>.
- St. George, S., 2014. An overview of tree-ring width records across the Northern Hemisphere. *Quat. Sci. Rev.* 95, 132–150. <https://doi.org/10.1016/j.quascirev.2014.04.029>.
- Stekhoven, D.J., Buhmann, P., 2012. MissForest—non-parametric missing value imputation for mixed-type data. *Bioinformatics* 28, 112–118. <https://doi.org/10.1093/bioinformatics/btr597>.
- Tardif, J., Camarero, J.J., Ribas, M., Gutiérrez, E., 2003. Spatiotemporal variability in tree growth in the Central Pyrenees: climatic and site influences. *Ecol. Monogr.* 73, 241–257.
- Truettner, C., Anderegg, W.R.L., Biondi, F., Koch, G.W., Ogle, K., Schwalm, C., Litvak, M.E., Shaw, J.D., Ziaco, E., 2018. Conifer radial growth response to recent seasonal warming and drought from the southwestern USA. *For. Ecol. Manag.* 418, 55–62. <https://doi.org/10.1016/j.foreco.2018.01.044>.
- Turcotte, A., Morin, H., Krause, C., Deslauriers, A., Thibeault-Martel, M., 2009. The timing of spring rehydration and its relation with the onset of wood formation in black spruce. *Agricultural and Forest Meteorology* 149, 1403–1409. <https://doi.org/10.1016/j.agrformet.2009.03.010>.
- Vaganov, E.A., Hughes, M.K., Kirdyanov, A.V., Schweingruber, F.H., Silkin, P.P., 1999. Influence of snowfall and melt timing on tree growth in subarctic Eurasia. *Nature* 400, 149–151. <https://doi.org/10.1038/22087>.
- van der Maaten, E., van der Maaten-Theunissen, M., Smiljanic, M., Rossi, S., Simard, S., Wilmingk, M., Deslauriers, A., Fonti, P., von Arx, G., Bouriaud, O., 2016. dendrometeR: Analyzing the pulse of trees in R. *Dendrochronologia* 40, 12–16. <https://doi.org/10.1016/j.dendro.2016.06.001>.
- Vapaavuori, E.M., Rikala, R., Ryypöä, A., 1992. Effects of root temperature on growth and photosynthesis in conifer seedlings during shoot elongation. *Tree Physiology* 10, 217–230.
- Watson, E., Luckman, B.H., 2016. An investigation of the snowpack signal in moisture-sensitive trees from the Southern Canadian Cordillera. *Dendrochronologia* 38, 118–130. <https://doi.org/10.1016/j.dendro.2016.03.008>.
- Woelber, B., Maneta, M.P., Harper, J., Jenesco, K.G., Gardner, W.P., Wilcox, A.C., López-Moreno, I., 2018. The influence of diurnal snowmelt and transpiration on hillslope throughflow and stream response. *Hydrol. Earth Syst. Sc.* 22 (8). <https://doi.org/10.5194/hess-22-4295-2018>.
- Zeide, B., 1993. Analysis of growth equations. *For. Sci.* 39, 594–616.
- Zhang, L., Axmacher, J.C., Sang, W., 2017. Different radial growth responses to climate warming by two dominant tree species at their upper altitudinal limit on Changbai Mountain. *J. For. Res.* 28, 795–804. <https://doi.org/10.1007/s11676-016-0364-5>.
- Zhang, T., 2005. Influence of the seasonal snow cover on the ground thermal regime: An overview. *Rev. Geophys.* 43. <https://doi.org/10.1029/2004RG000157>.
- Zhang, X., Manzanedo, R.D., D'Orangeville, L., Rademacher, T.T., Li, J., Bai, X., Hou, M., Chen, Z., Zou, F., Song, F., Pederson, N., 2019. Snowmelt and early to mid-growing season water availability augment tree growth during rapid warming in southern Asian boreal forests. *Glob. Change Biol.* 25, 3462–3471. <https://doi.org/10.1111/gcb.14749>.
- Zweifel, R., Item, H., Hässler, R., 2000. Stem radius changes and their relation to stored water in stems of young Norway spruce trees. *Trees* 15, 50–57. <https://doi.org/10.1007/s004680000072>.